
Jaziri, Nesrine; Boughamoura, Ayda; Müller, Jens; Mezghani, Brahim;
Tounsi, Fares; Ismail, Mohammed:

A comprehensive review of thermoelectric generators: technologies and common applications

<i>Original published in:</i>	Energy reports. - Amsterdam [u.a.] : Elsevier. - 6 (2020), Supplement 7, p. 264-287.
<i>Original published:</i>	2019-12-24
<i>ISSN:</i>	2352-4847
<i>DOI:</i>	10.1016/j.egyr.2019.12.011
<i>[Visited:</i>	2021-02-22]



This work is licensed under a [Creative Commons Attribution 4.0 International](https://creativecommons.org/licenses/by/4.0/) license. To view a copy of this license, visit <https://creativecommons.org/licenses/by/4.0/>



Review article

A comprehensive review of Thermoelectric Generators: Technologies and common applications



Nesrine Jaziri ^{a,b,c,*}, Ayda Boughamoura ^d, Jens Müller ^b, Brahim Mezghani ^a, Fares Tounsi ^a, Mohammed Ismail ^e

^a Micro Electro Thermal Systems (METS) Group, Ecole Nationale d'Ingénieurs de Sfax (ENIS), Université de Sfax, 3038, Sfax, Tunisia

^b Electronics Technology Group, Institute of Micro and Nanotechnologies MacroNano, Technische Universität Ilmenau, Germany, Gustav-Kirchhoff-Straße 1, 98693, Ilmenau, Germany

^c Université de Sousse, Ecole Nationale d'Ingénieurs de Sousse, 4023, Sousse, Tunisia

^d Université de Monastir, Ecole Nationale d'Ingénieurs de Monastir (ENIM), Laboratoire d'Etude des Systèmes Thermiques et Energétiques (LESTE), LR99ES31, 5019, Monastir, Tunisia

^e Department of Electrical and Computer Engineering, College of Engineering, Wayne State University, Detroit, MI48202, USA

ARTICLE INFO

Article history:

Received 18 July 2019

Received in revised form 7 December 2019

Accepted 10 December 2019

Available online 24 December 2019

Keywords:

Thermoelectric generator
MEMS/LTCC technologies
Wearable devices
WSNs
Biomedical
Vehicle engine
Aerospace

ABSTRACT

Power costs increasing, environmental pollution and global warming are issues that we are dealing with in the present time. To reduce their effects, scientists are focusing on improving energy harvesting-based power generators. Thermoelectric generators (TEGs) have demonstrated their ability to directly convert thermal energy into an electrical one via the Seebeck effect. Also, they are environmentally friendly because they do not contain chemical products, they operate silently because they do not have mechanical structures and/or moving parts, and they can be fabricated on many types of substrates like silicon, polymers, and ceramics. Furthermore, TEUs are position-independent, present a long operating lifetime and are suitable for integration into bulk and flexible devices. This paper presents in-depth analysis of TEUs, starting by an extensive description of their working principle, types (planar, vertical and mixed), used materials, figure of merit, improvement techniques including different thermoelectric materials arrangement (conventional, segmented and cascaded), and used technologies and substrates types (silicon, ceramics and polymers). This manuscript also describes the exploitation of TEUs in various fields starting from low-power applications (medical and wearable devices, IoT: internet of things, and WSN: wireless sensor network) to high-power applications (industrial electronics, automotive engines, and aerospace).

© 2019 The Authors. Published by Elsevier Ltd. This is an open access article under the CC BY license (<http://creativecommons.org/licenses/by/4.0/>).

Contents

1. Introduction.....	264
2. Thermoelectric generators basis.....	265
2.1. Main design approaches.....	265
2.2. Fabrication technologies.....	266
2.3. Figure of merit and thermocouples arrangement.....	266
3. Common applications	270
3.1. In medical and wearable devices.....	270
3.2. In wireless sensor networks.....	271
3.3. In industrial electronic devices.....	274
3.4. In automobile engines.....	276
3.5. In aerospace.....	279
4. Conclusion	282
Declaration of competing interest.....	284
References	284

1. Introduction

The uses of natural gas, fuel, and coal to generate electricity have become detrimental for human-beings because of their

* Corresponding author.

E-mail address: nesrine.jaziri@tu-ilmenau.de (N. Jaziri).

adverse effects on atmospheric pollution and global warming. Nevertheless, according to the US Energy Information Administration (EIA), electricity generated from power plants using natural gas was increasing every year with 28% in 2014, 35% in 2018 and 36% in 2019 (U.E.I. Administration, 2018). Furthermore, the world consumption and production of liquid fuels increased from 94 million barrels per day in mid-2014 to 100 million in mid-2018, which is leading to an ever-increasing energy cost. To cope with this global growth in the consumption of fossil fuels, quite expensive and polluting, other forms of environment-friendly energies arose in the last decades. Indeed, Nicolas Tesla once said: “*Electric power is everywhere present in unlimited quantities and can drive the world's machinery without the need of coal, oil, gas or any other of the common fuels*”. This quote anticipates the current new trend of harvesting natural energy from the environment to provide unlimited, sustainable, green and cheap electrical power. Nowadays the growing interest in using renewable energy, that can be scavenged from several natural abandoned sources such as RF radiation, thermal, solar, vibratory/mechanical energy, etc., and converting it into electrical one to supply the world's electronic devices and machinery, is growing exponentially.

Thermal energy is one of the abundantly available energies that could be found in many sectors like in operating electronic devices (integrated circuits, phones, computers, etc.), running vehicles, in-door buildings, and even in human body (*in-vivo*). Thermoelectric generators (TEGs) are active devices that consist of converting thermal energy into electrical one (Proto et al., 2018). TEGs are made of dissimilar thermocouples, based on the Seebeck effect, connected electrically in series and thermally in parallel. TEGs are widely used in many fields due to their attractive features, such as energy efficiency, free maintenance and long lifetime. Throughout the last years, they have become an area of interest in the field of energy harvesting for large and even small types of applications, depending on size, delivered power and used materials.

In this paper, we will present a comprehensive state of the art of TEGs. This paper differs from other reviewing papers (Siddique et al., 2017; Patil et al., 2018) in presenting the different types (planar, vertical and mixed) and technologies (silicon, ceramics, and polymers) of TEGs. We will also investigate the latest thermoelectric materials and keys for generating high-efficient power factor with the different TE materials arrangement (conventional, segmented and cascaded). Furthermore, we will present the use of TEGs in high and low-power applications (medical, wearable, IoT, WSN, industrial electronics, automobiles and aerospace applications).

2. Thermoelectric generators basis

Thermoelectric generators are based on the Seebeck effect and are commonly used to convert thermal energy into an electrical one. TEGs provide many advantages such as design simplicity, the absence of moving parts, long lifetime, unnecessary maintenance and environmental friendliness (does not contain chemical products). TEGs are usually made of many connected thermopiles in order to increase the output power (Leonov et al., 2007; Markowski, 2016). Each thermopile is made of many thermocouples (TCs) connected electrically in series and thermally in parallel (Fig. 1a). The thermocouple is made with two different materials, having an opposite Seebeck coefficient, joined at their ends. Due to Seebeck effect, the appearance of a temperature gradient, $\Delta T = T_{\text{hot}} - T_{\text{cold}}$, between the two TCs ends, generates an electric voltage expressed as (Yang et al., 2013; Pasquale, 2013):

$$V_{\text{out}} = N\alpha_{AB}\Delta T \quad (1)$$

where N is the number of connected thermocouples, α_{AB} is the Seebeck coefficients of the two joined materials A and B forming the thermocouple ($\alpha_{AB} = \alpha_A - \alpha_B$). When the TCs are connected electrically in series, the total internal resistance is proportional to their number N . So, even though a high number of TCs will increase the voltage delivered by the TEGs, its impact on the internal resistance is adverse (Fig. 1b). Indeed, the increases of series connected TCs number will lead to a rise of the TEG's internal resistance which is expressed as (Wang et al., 2013):

$$R_{\text{TEG}} = N \left(\frac{\rho_A L_A}{S_A} + \frac{\rho_B L_B}{S_B} + 2 \frac{\rho_C L_C}{S_C} \right) \quad (2)$$

where ρ_A , ρ_B and ρ_C are, respectively, the electrical resistivity of the materials A, B and the metallic contact. L_A and L_B are the thermocouple arms lengths crossed by the heat flow, and L_C is the contact length. S_A , S_B and S_C are, respectively, the A and B thermocouples and contacts cross-sectional areas. The delivered output power of the generator is given by:

$$P = V_{\text{out}}^2 \frac{R_L}{(R_{\text{TEG}} + R_L)^2} \quad (3)$$

where R_L and R_{TEG} are, respectively, the external load and the internal resistances (Fig. 1b). If the load resistance is matching the internal TEG's resistance, R_{TEG} , the maximum output power is expressed as:

$$P_{\text{max}} = \frac{V_{\text{out}}^2}{4R_{\text{TEG}}} \quad (4)$$

2.1. Main design approaches

There are three design approaches of TEGs which differs according to the thermocouples' arrangement on the substrate regarding the heat flow direction (Glatz et al., 2009), which are: (i) Lateral heat flow, lateral TCs arrangement; (ii) Vertical heat flow, vertical TCs arrangement; and (iii) Vertical heat flow, lateral TCs arrangement.

The first TEG design uses a lateral TCs arrangement to convert a lateral heat flow, Q_h-Q_c . In this design, called also planar TEG, thermocouples are printed, patterned or deposited on the substrate surface (Fig. 2a). The main advantage of this approach lies in its ability to manipulate the thickness and the length of each thermocouple arm combined to its suitability with thin film deposition, which allows creating thinner and longer thermocouples compared to other types (Glatz et al., 2009; Kao et al., 2010; Qing et al., 2018). Besides, this arrangement increases the thermal resistance of the thermoelements compared to other TEGs designs because of using lengthy TCs arms which leads to a temperature gradient increasing along these latter, and eventually an output voltage rising.

The second TEG design, i.e. vertical TEG, is made of TCs arranged vertically between the heat source and the heat sink (Fig. 2b) (Aravind et al., 2018). Thus, the heat is flowing vertically along the thermoelement arms and the substrates. This arrangement is similar to the Peltier-based module for refrigeration. This kind of TEGs provides high integration density, and is the most commercialized because of its simplicity, high TCs integration, and high output voltage (Leonov, 2013).

The last TEG design, referred to as mixed, is made by TCs mounted laterally on the substrate, while the heat flows vertically (Fig. 2c) (Sawires et al., 2018; Yan et al., 2019; Huu et al., 2018). The vertical heat transfer was instigated through the integration of micro-cavities into the substrate, located under the thermocouple arms (Ziouche et al., 2017). This technique could be achieved in silicon when using CMOS standard technology, or by a lift-off process in polyimide/polymer-based flexible foil. This latter

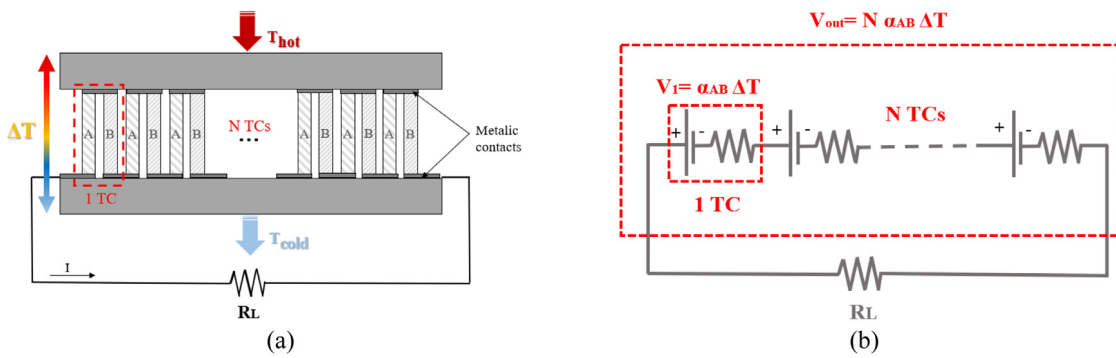


Fig. 1. Typical thermoelectric generator: (a) Basic principle, (b) Equivalent electrical circuit.

consists of creating a wavy form in the substrate containing the patterned thermocouples (Hasebe et al., 2004). The second and the third TEG designs should include two extra plates/substrates placed above and beyond the hot and cold sides of the module. In this case, the thermal conductivity of the substrate will influence the temperature difference of the module especially when it is much lower than that of thermocouples. This will decrease the temperature difference between the TC arms. The temperature difference between the thermocouples is changed as (Sawires et al., 2018):

$$\Delta T_{TE} = \frac{\theta_{TE}}{\theta_{TE} + \theta_h + \theta_c} \Delta T_{TEG} \quad (5)$$

where, ΔT_{TEG} is the temperature difference between the two substrates, and θ_{TE} , θ_h and θ_c are respectively the thermal resistances of the thermocouples, the hot and the cold plates.

2.2. Fabrication technologies

TEGs could be fabricated using different kinds of technologies, using a variety of fabrication methods, on different hosting substrate materials, such as:

- Silicon technology (with CMOS-IC or CMOS-MEMS technologies) (Yang et al., 2013; Kao et al., 2010; Ziouche et al., 2017; Chen et al., 2018), serves to create small-scale generators (dimensions in the order of micro- to nano-meters) (Fig. 3). Both compatible (such as N- and P-type polycrystalline silicon, poly-SiGe and recently silicon nanowires (SiNW) (Li et al., 2011b; Zhang et al., 2018)) and non-compatible CMOS materials like Bi-Sb-Te alloy (Li et al., 2003; Nurnus, 2007; Völklein and Megier, 2006; Völklein et al., 1999) have been used for the fabrication of the TC arms. CMOS technology allows also the creation of micro-cavities in the silicon substrate to prevent heat dissipation under the hot junctions as shown in Fig. 3 (Chen et al., 2018; Ziouche et al., 2017).

- Alumina (Al_2O_3)- and Low-Temperature Co-fired Ceramic (LTCC)-based technologies allow creating a multilayered approach for high-density TEGs (Markowski, 2016; Markowski and Dziedzic, 2008; Markowski et al., 2008; Markowski, 2011, 2014). Indeed, exploiting ceramics technology in TEG's fabrication will be advantageous thanks to its multilayered deposition capability, simplicity, low-cost, time effectiveness and good resistance in harsh environments, like in high temperatures, gases, and stresses (Thelemann et al., 2002; Gongora-Rubio et al., 2001; Gierth et al., 2018). In ceramic-based technologies, thermocouples could be fabricated using thick (Markowski and Dziedzic, 2008; Markowski, 2014, 2011, 2016), thin (Markowski et al., 2015) and mixed (thick/thin) (Markowski et al., 2009; Gierczak et al., 2017, 2018) deposition techniques. Thick film-based thermocouples are fabricated using a screen-printing technique with plenty of different material pastes such as Ag, PdAg, Ni, Pt, Al, W, and Pd. Thin

films are fabricated using various deposition techniques from the microelectronic industry using metals and semiconductor materials like Germanium-based compositions (Markowski et al., 2009; Markowski et al., 2015), and group III-Nitride alloys like Aluminum Nitride (AlN) and Gallium Nitride (GaN) (Mánel et al., 2018; Jiménez et al., 2019). Thin-film, on ceramic, based semiconductor materials present a high Seebeck coefficient but they also present very high electrical resistivity. Furthermore, ceramic substrates possess low thermal conductivity compared to silicon ones, about 3.3 W/K.m for the DP951 green tape, which provides an important thermal resistance of the ceramic-based generator. This leads thereafter to a high-temperature gradient along the LTCC-based TEG and results in a significant output voltage. Ceramic based substrates are most suitable for lateral TEG's design (Fig. 4a) to decrease heat transfer between the TC arms and obtain a higher temperature difference between the hot and cold junctions. For vertical TEG's design, this technology could be presented by fabricating the TC arms vertically along the substrate by punching several vias in the substrate and filling them with conductive paste in order to obtain vertical TCs arrangement (Fig. 4b) (Markowski and Dziedzic, 2008).

- Polymers—(Fig. 5a) (Huu et al., 2018; Hasebe et al., 2004; Suarez et al., 2017b), polyimide—(PI) (Fig. 5b) (Park et al., 2017), even cellulose fibers-based (Fig. 5c) (Zhu et al., 2018), and Fabric (Fig. 5d) (Elmoughni et al., 2019) substrates are the most appropriate for creating flexible TEGs (f-TEGs) for wearable applications. The used techniques include screen-printing for thick films, and electro-deposition, sputtering or evaporation for thin films fabrication.

Table 1 summarizes the latest TEG structures, types and output parameters when using different technologies, substrates, and materials.

2.3. Figure of merit and thermocouples arrangement

Many conductive and semiconductor materials are used in thermocouples fabrication. However, it is necessary to carefully choose among these materials to obtain better electrical performances, i.e. high output voltage, low internal electrical resistance, and high electrical power. The appropriateness of a thermoelectric (TE) material is evaluated through its figure of merit, Z, reflecting its quality factor, and is expressed as:

$$Z = \frac{\alpha^2}{\rho \lambda} \quad (6)$$

where α , ρ and λ are respectively the Seebeck coefficient [V/K], the electrical resistivity [$\Omega \text{ m}$] and the thermal conductivity [W/(K m)] of the material. The figure of merit allows knowing the efficiency of a thermoelectric material during the conversion of the heat into electricity. However, the higher this factor is, the

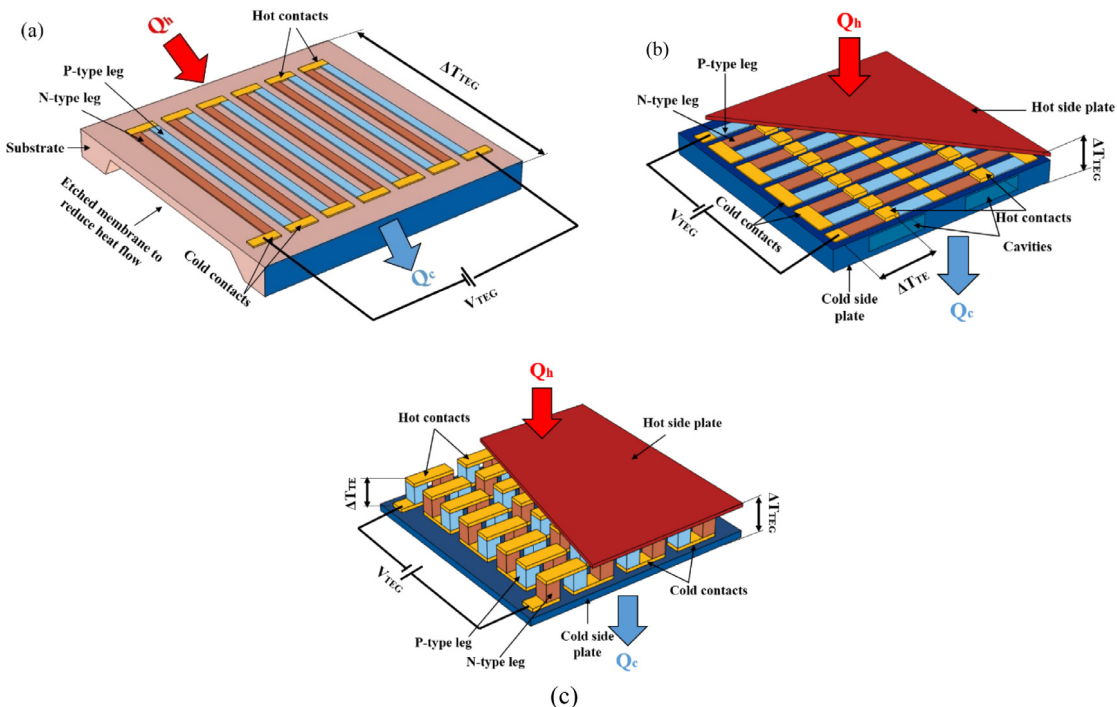


Fig. 2. Different TEGs designs: (a) Planar, (b) Vertical, and (c) Mixed.

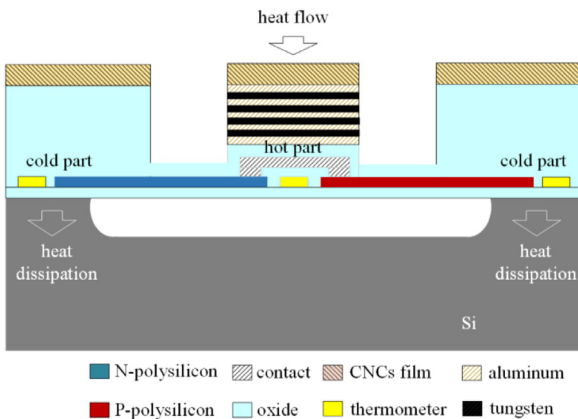


Fig. 3. Cross-section schematic illustration of a mixed TEG with N- and P-types polysilicon thermocouples fabricated with CMOS technology showing a suspended hot part (Chen et al., 2018).

more the material is efficient. Furthermore, the figure of merit is a temperature-dependent and each material present its high figure of merit in a certain range of temperature. For one TE material, the dimensionless figure of merit is expressed as (Kim et al., 2015; Snyder and Snyder, 2017):

$$ZT = \frac{\alpha^2}{\rho \lambda} T \quad (7)$$

where T is the absolute temperature of the material [K]. For a TE couple composed of A and B materials, the dimensionless figure of merit is defined as (Simon, 1961; Goldsmid et al., 1985):

$$(ZT)_{AB} = \frac{\alpha_{AB}^2}{[(\rho_A \lambda_A)^{0.5} + (\rho_B \lambda_B)^{0.5}]^2} T \quad (8)$$

For a module of N thermocouples, ZT of the whole thermogenerator can be formulated as (Thielen et al., 2017):

$$(ZT)_{TEG} = \frac{(N\alpha_{AB})^2}{R_{TEG} K_{TEG}} T \quad (9)$$

where K_{TEG} is the thermal conductance of the generator and R_{TEG} is the internal electrical resistance. The energy conversion

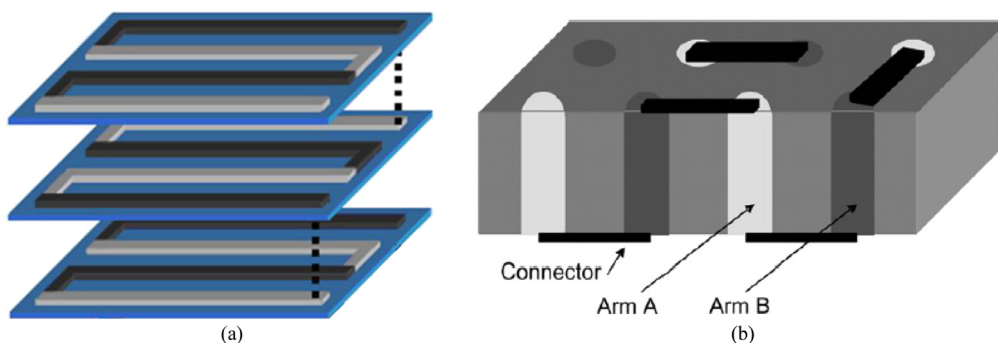


Fig. 4. LTCC-based multilayered TEG, (a) Planar design using Ag/Ni thermocouples (Markowski, 2016), (b) Vertical design using conductive vias (Markowski and Dziedzic, 2008).

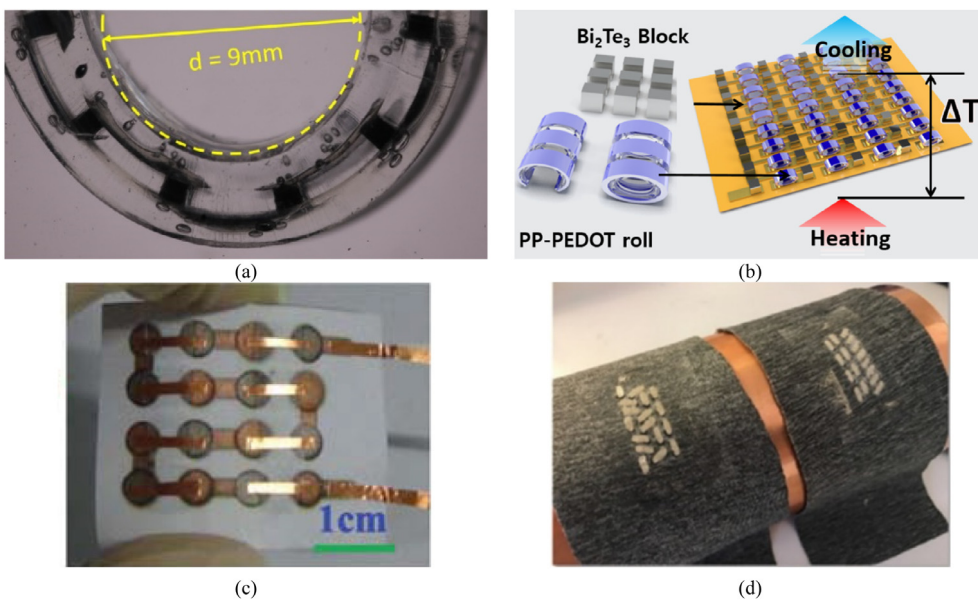


Fig. 5. Vertical flexible TEGs fabricated on a substrate made of: (a) PDMS polymer ([Suarez et al., 2017a](#)), (b) Polyimide (PI) ([Park et al., 2017](#)) , (c) Cellulose fiber (paper substrate with cooper/nickel TCs) ([Zhu et al., 2018](#)), and (d) Knitted fabric ([Elmoughni et al., 2019](#)).

efficiency of a generator, also called thermoelectric conversion efficiency, is expressed as ([Hussain et al., 2009](#)):

$$\eta = \frac{P}{Q_h} \quad (10)$$

where P is the produced electrical power from the generator and Q_h is the incoming heat flow at the hot side of the TEG. It is expressed as:

$$\dot{Q}_h = \lambda \Delta T + \alpha T_h I - \frac{1}{2} I^2 R \quad (11)$$

The maximum conversion efficiency could be expressed in function of the Carnot efficiency ($(T_h - T_c)/T_h$) and the dimensionless figure of merit factor of the used materials as ([Kim et al., 2015](#); [Snyder and Snyder, 2017](#)):

$$\eta_{max} = \frac{T_h - T_c}{T_h} \frac{(\sqrt{1 + ZT_{AB}} - 1)}{\sqrt{1 + ZT_{AB}} + T_c/T_h} \quad (12)$$

As the conversion efficiency is related to the figure of merit, good thermoelectric materials should present a high Seebeck coefficient, low electrical resistivity, and low thermal conductivity. Since metals present low electrical resistivities, high thermal conductivities, and low Seebeck coefficients, they engender a low figure of merit. Contrariwise, the highest figure of merit belongs to the semiconductors class. The most used thermoelectric materials are Bi_2Te_3 , PbTe and CoSb_3 providing ZT around 1 ([Hébert, 2014](#); [Beltrán-Pitarch et al., 2018](#); [Shu et al., 2018](#)).

Recently, researchers are focusing on the industrialization of novel thermoelectric materials with a higher figure of merit. However, one of the core problems that restrict achieving materials with a high figure of merit is the dependency of the Seebeck coefficient and electrical conductivity, where increasing the Seebeck coefficient leads to the carrier concentration decreasing and then the decreasing of the electrical conductivity. Also, difficulties in minimizing heat losses during the determination of thermal conductivity considered as one of the main problems ([Beltrán-Pitarch et al., 2018](#)). However, researchers succeeded in synthesizing some materials, such as Cu_{2-x}Se , and $\text{PbTe}_{0.7}\text{S}_{0.3}$, with a figure of merit $ZT > 2$ ([Olvera et al., 2017](#); [Wu et al., 2014](#)).

Since thermoelectric materials properties are temperature dependent, they usually present the highest ZT under certain temperature range. Hence, to achieve maximum benefit, recent studies are focusing on designing and fabricating thermocouples with segmented materials based on the operating temperature in order to endure the required heat source's temperature while maintaining the highest ZT ([Shu et al., 2018](#); [Tian et al., 2015](#); [Ge et al., 2018](#)). [Fig. 6](#) presents the difference between ordinary and segmented thermocouple arrangements ([Shu et al., 2018](#)). The TE materials in segmented TEGs structure are arranged according to their optimal operating temperature range, from high to low temperatures. [Table 2](#) presents the TE materials properties according to their optimal operating temperature range.

However, heterogeneity between different stacked materials, with different mechanical properties, especially thermal expansion coefficients, mechanical stresses, thermal and chemical stability, may affect the compatibility of the segmented materials and then reduce the maximum thermoelectric efficiency (η_{max}). The maximum TE efficiency is only achieved when the relative current density is equal to the compatibility factor for all segmented materials ([Snyder and Ursell, 2003](#); [Snyder, 2004](#)). The compatibility factor, s, and the relative current density, u, are respectively given by:

$$s = \frac{\sqrt{1 + ZT} - 1}{\alpha T} \quad (13)$$

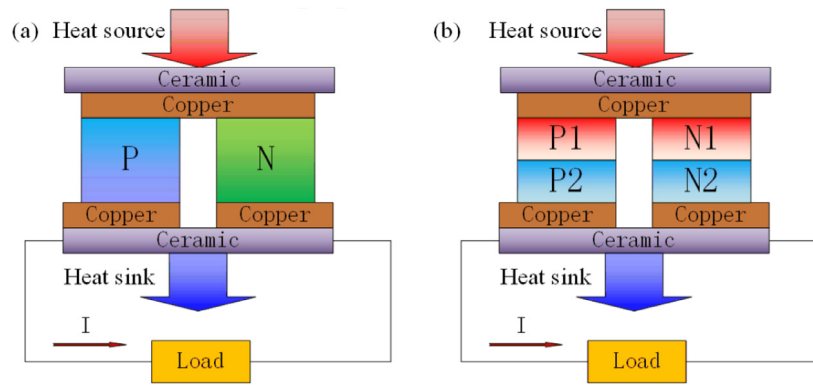
$$u = \frac{J}{\lambda \nabla T} \quad (14)$$

Consequently, to solve the incompatibility problem, an appropriate cascaded approach of the different TE materials arrangement is needed ([Zhang et al., 2008](#); [Gou et al., 2017](#); [Kanimba et al., 2017](#)). This approach is based on arranging TCs in different stages (mounting in a parallel way). Each stage is connected independently to the load circuit. The electrical connectivity's self-reliance in each stage for the cascaded arrangement allows the independency of the electrical, mechanical and thermal properties which will beget higher materials' efficiency. [Fig. 7a](#) presents two stages of TCs arrangement. [Fig. 7b](#) presents three stages TE modules arrangement. The selection of TE materials and type of arrangement, depending on the application's environment, will be discussed in the next section. Moreover, another core problem

Table 1

Summary of TEGs structures, types and output parameters based on different technologies/substrates.

Substrate	TEG's type	TCs materials	Techniques	# of TCs	TCs lengths [mm]	TCs area [mm ²]	Max ΔT [K]	V _{TEG} [mV]	P _{TEG} [μW]	Year & Ref
Silicon	Si + thin PCB layer	Vertical	Poly-SiGe	Surface micro-machining (with LPCVD TCs deposition)	2350–4700	0.003	–	50	150	0.0003 2009 (Wang et al., 2009)
	Si	Planar	N and P types poly-Si	0.35 μm CMOS process (with CVD TCs deposition)	33	0.64	0.005 × 0.0003	1	0.067	4.8E–7 2010 (Kao et al., 2010)
				0.35 μm CMOS process (with CVD TCs deposition)	24	0.12	0.008 × 0.0002	15	0.55	9.4 2013 (Yang et al., 2013)
		Mixed	N-type poly-Si/Au	Monolithic CMOS process (with LPCVD TCs deposition)	560	1	–	31,5	4,1	4,2 2017 (Ziouche et al., 2017)
Ceramic	LTCC		N and P types poly-Si	CMOS-UMC 0.13μm 1P8M process	273870	0.019	0.004 × 0.00016	2.34	–	9.25 2018 (Sawires et al., 2018)
		Vertical	Ag/Ni	Needle + compressed air	18	1.75	5.49	18	4.8	0.8 2008 (Markowski and Dziedzic, 2008)
		Planar	PdAg/TSG	– Screen printing	35	7	0.2 × 0.01 0.2 × 0.003	100	660	5. 6 2009 (Markowski et al., 2009)
		Planar	Ag/WSG	– Magnetron sputtering			0.2 × 0.02 0.2 × 0.003	100	700	19.6 2014 (Markowski, 2014)
		Planar	Ag/PdAg	Screen printing	450	14.1	0.13 × 0.005 0.13 × 0.009	135	450	130 2016 (Markowski, 2016)
		Planar	Ag/Ni	Screen printing	90	17	0.15 × 0.0155 0.15 × 0.012	193	353	460 2017 (Gierczak et al., 2017)
Polymer	Alumina (96% Al ₂ O ₃)	Planar	Ag/Cu-Ni alloy	- Screen printing - Magnetron sputtering	16	27	0.315 × 0.02.8 0.3 × 0.012	85	57	– 2019 (Yuan et al., 2019)
	PI	Planar	Sb ₂ Te ₃ /Bi ₂ Te _{2.7} Se _{0.3}	Screen printing	150	5.5	–	48	2.2E3	150 2019 (Zhao et al., 2019)
	Paper	Vertical	Bi _{0.5} Sb _{1.5} Te ₃ /Bi ₂ Se _{0.3} Te _{2.7}	Pipette + Plate pressing	10	0.2	15.07	35	8.3	10 2019 (Elmoughni et al., 2019)
Fabric			PEDOT:PSS/Na(NiETT)	Stencil printing	32	0.5	6.9	3	3	0.5 2019 (Elmoughni et al., 2019)

**Fig. 6.** Thermoelectric materials arrangements for (a) Conventional thermocouple, (b) Segmented thermocouple (Shu et al., 2018).

that restricts the progress of achieving high-efficient thermoelectric materials is the high cost of their development which also

results in a high industrialization cost. For instance, the Bismuth (III) telluride (Bi₂Te₃), the BiSb and Skutterudites (e.g. CoSb) cost,

Table 2

Classification of TE materials according to their operating temperature (Li et al., 2011a; LaGrandeur et al., 2006; Espinosa et al., 2010).

Group	Material	Best temperature range (K)	Peak ZT
High Temperature (HT) (700–1000 K)	CoSb ₃ (n-type)	650–1100	0.9
	PbTe (n-type)	600–850	0.8
	SiGe (n-type)	>1000	0.9
	Zn ₄ Sb ₃ (p-type)	>600	1.4
	CeFe ₄ Sb ₁₂ (p-type)	>850	1.5
	SiGe (p-type)	900–1300	0.5
	TAGS (p-type)	650–800	1.3
	CeFe ₃ RuSb ₁₂	—	—
Medium Temperature (MT) (400–700 K)	Mg ₂ Si (n-type)	645	1.1
	Tl ₉ BiTe ₆ (p-type)	>400	1.3
Low Temperature (LT) (300–400 K)	Bi ₂ Te ₃ (n-type)	<350	0.7
	Bi ₂ Te ₃ (p-type)	<450	1.1
	(Bi,Sb) ₂ Te ₃ (p-type)	375	1

respectively, about 1278 \$/100 g, 1830 \$/100 g, and 3946.5 \$/100 g (Sigma-Aldrich, 2019). However, improving TE materials will increase the TEG's conversion efficiency.

3. Common applications

TEGs are widely used in many applications such as automobile engines (Crane and LaGrandeur, 2010; Orr et al., 2017; Cao et al., 2018; Mostafavi and Mahmoudi, 2018), industrial electronic devices (Solbrekken et al., 2004; Zhou et al., 2008), micro self-powered wireless platforms (Guan et al., 2017; Musleh et al., 2017), health monitoring and tracking systems (Amar et al., 2015; Torfs et al., 2006; Thielen et al., 2017), and aerospace (Liu et al., 2017; Yuan et al., 2018). These applications require different sizes and supplying powers. Thereby, TEGs are divided into two types, large (or bulk) and micro-TEGs. The first category has a millimetric dimension and provides output power from several to hundreds of Watts under a high heat range. This category is usually used for industrial purposes. The second category works with low wasted heat and generates electrical power in the range of μW to a few mW (Liu et al., 2018a). In the next subsections, we will introduce TEGs used in these different kinds of applications.

3.1. In medical and wearable devices

Since body heat is a sustainable energy, it can be exploited to supply fully of emerging wearable and implanted medical devices (IMDs) allowing a various range of applications such as health monitoring and tracking systems, sports and fitness wearable devices, etc. Wahbah et al. (2014), Yang et al. (2007), Amar et al. (2015), Torfs et al. (2006), Thielen et al. (2017). These wireless medical devices/sensors can easily control safety and physiological conditions, health, and emergent issues and overall analysis of the patient in the hospital or at home. Body heat can act as a thermal engine to power these smart devices. Furthermore, wearable medical devices are not only specified for patients but also healthy people for a permanent examination during sports or even normal daily routine for calories and sleeping hours tracking. The amount of heat varies from 27.1 °C to 35.2 °C depending on body activities, location, and environmental conditions (Proto et al., 2018; Stark, 2011). Hence the average temperature gradient between the body and the ambient air is around 13 °C. The needed electrical power to supply wearable medical devices and IMDs is lower than 5mW (Pistoia, 2005). Using TEGs in medical devices and sensors is a suitable solution; especially for implantable medical devices where the maintenance (changing batteries) is a very costly and

time-consuming task (e.g. the surgery cost of an implantable cardioverter-defibrillator is \$8.250 without including the device price or the used batteries (Lind, 2017)). Furthermore, even when using rechargeable batteries (like lithium-ion batteries), they may cause hazardous results like over-heating caused by the battery over-charging. Fig. 8 presents some TEGs-based wearable applications. In these designs, TEGs are ideally placed vertically between the body skin (heat source) and the ambient air (heat sink) as shown in Fig. 8a.

Torfs et al. have successfully presented a wearable autonomous pulse oximeter to control oxygen saturation powered by body heat TEG in a wearable watch (Fig. 8b) (Torfs et al., 2006, 2007). The used commercial BiTe-based TEG generates 100 μW of electrical power at 22 °C, whereas the whole wireless system consumes only 62 μW . Van Bavel et al. have presented TEG-powered wireless electroencephalography (EEG) headband for recording the electrical activities of the brain (Fig. 8c) (Bavel et al., 2008; Leonov et al., 2009). The fabricated TEG generates 2–2.5 mW of electrical power, while the whole system consumes 0.8 W. In addition to conventional wearable devices, TEGs have also been used in wearable textiles and garments (Leonov, 2013; Myers and Jur, 2017; Leonov and Vullers, 2009b,a; Leonov et al., 2011). Leonov et al. have fabricated a planar CMOS-based TEG located between the skin and a T-shirt (Leonov et al., 2011). The fabric was acting like a flexible radiator. The bulk-micromachined TEG contains 1700 poly-Si thermocouples and produces >1 mW at the temperature of 11–13 °C, and generates an electrical voltage of 2 V. Leonov had also presented 8 TEGs for powering implanted electrocardiography (ECG) systems in wearable textiles (Leonov, 2013) (Fig. 8d). The used TEG presents a figure of merit $Z = 0.0025 \text{ K}^{-1}$ and generates 0.5–5 mW at a room temperature of 15–27 °C. From body heat generation, "Matrix Power Watch" is the first commercialized IoT smart-watch monitoring powered by a TEG (Fig. 8e) (Brewster, 2016; Boukai, 2017). No indication was provided about the fabrication technology of the proposed TEGs in this commercialized smart-watch. Fig. 8f presents the use of TEGs to supply a medical hearing prosthesis (Lay-Ekuakille et al., 2009). A thin-film-based TEG named MPG-D602, from Micropelt, has been used in this device.

On the other hand, μ -TEGs based on silicon-nanowires are becoming an area of interest in the field of high-power TEGs. They are compatible with CMOS technology and have a low thermal conductivity, low fabrication cost, and higher simplicity. Watanabe et al. studied the influence of the Si-nanowires length on the μ -TEGs electrical parameters (Watanabe et al., 2017). They also developed a new scaled design with shorter thermocouples length arranged in series between hot-side and cold-side conductors. This μ TEG consists of suspended 0.25 μm -width P- and

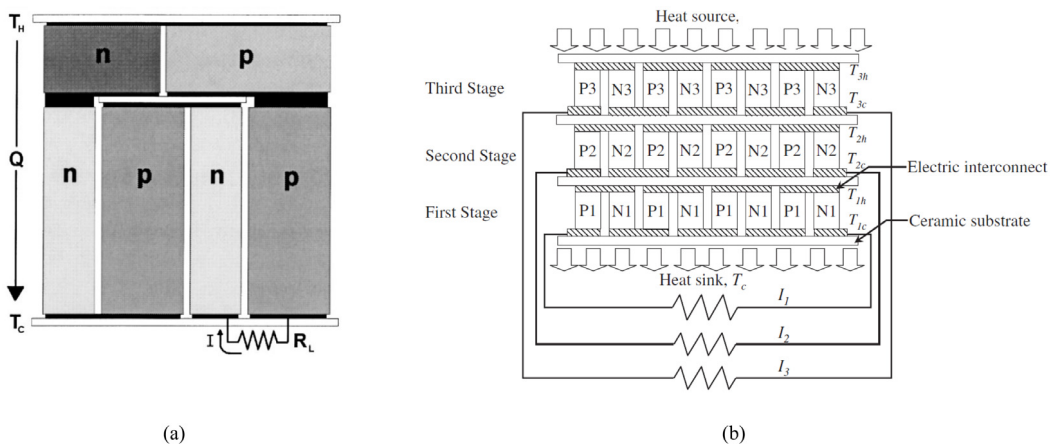


Fig. 7. Cascaded arrangement of TE materials: (a) Two stages cascaded design (Snyder, 2004), (b) Three stages cascaded TE module (Zhang et al., 2008).



Fig. 8. Wearable vertical TEG applications: (a) schematic illustration of a TEG module powered by body heat with (1) thermal interface between skin/TEG's hot side, (2) TEG module, and (3) heat sink providing heat dissipation to the ambient air (Thielen et al., 2017), (b) Wearable pulse oximeter based on CMOS-based TEG with poly-SiGe TCs (Leonov et al., 2009), (c) Electroencephalography (EEG) headband (Leonov et al., 2009), (d) electrocardiography (ECG) shirt (Leonov, 2013), (e) Matrix Power Watch powered by TEG and body heat (Boukai, 2017), and (f) Biomedical hearing aid (Lay-Ekuakille et al., 2009).

N-type silicon nanowires on an SOI-wafer of 50 μm -thickness. Fig. 9a and b present the difference between the conventional and the scaled μ TEG. The planar scaled silicon-nanowire μ TEG was designed with 400 Si-NWs which were fabricated by a dry etching technique and electron beam lithography with 100 nm of Si-wire's width and 8–90 μm length (Fig. 9c). The results show that the maximum power ($\approx 1000 \text{ pW}$) and lower internal resistance ($\approx 0.3 \text{ k}\Omega$) were related to the shortest leg's length ($L = 8 \mu\text{m}$) (Fig. 9d). Improving the efficiency of such novel high-power Si-nanowires-based μ TEG, manufactured with CMOS-IC technology, presents an outstanding achievement Tomita et al. (2018). The latter generates 12 $\mu\text{W}/\text{cm}^2$ of power density for just 5 $^\circ\text{C}$ of a temperature gradient.

Huu et al. (2018) presented a human body-powered lateral Y-type flexible thermoelectric generator (f-TEG) based on an electrochemical deposition. The f-TEG was fabricated using N-type bismuth telluride (Bi_2Te_3) and P-type antimony telluride (Sb_2Te_3) thick films on a flexible $1 \times 1 \text{ cm}^2$ polymer substrate (Fig. 10a and b). The fabricated f-TEG made it possible to generate 56 mV of electric voltage and 3 $\mu\text{W}/\text{cm}^2$ of electrical power density under 37 $^\circ\text{C}$ of body heat temperature and 15 $^\circ\text{C}$ of environment

ambient temperature. Fig. 10c presents the output power density versus the applied body heat temperature of the Y-type flexible TEG.

3.2. In wireless sensor networks

Wireless Sensor Networks (WSNs) have become rapidly a field of interest during the last three decades. It combines wireless communication with the use of smart and advanced sensors network. Exploiting TEGs for self-powering WSNs helps in reducing maintenance tasks and costs neglects the utilization of batteries and reduces environmental pollution from chemical products emitted from them (Dilhac et al., 2014). This technology, combined with TEGs, has been applied in many areas like Building Energy Management (BEM) (Wang et al., 2013), industry (Kim et al., 2018; Jezzi et al., 2017), commercial and residential smart-buildings (Guan et al., 2017; Musleh et al., 2017) where heating sources like heat pipes, water heaters, central heating, and air conditioners are widely existing. Also, introducing TEGs-based self-powered WSNs are used in aeronautical

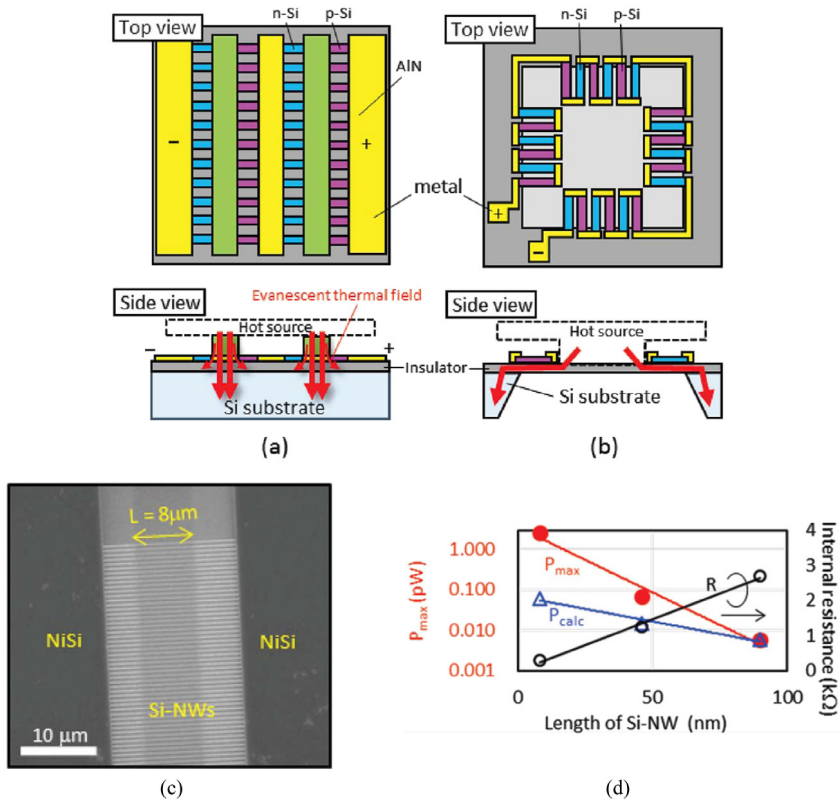


Fig. 9. Si-NWs planar TEG (a) Scaled TEG, (b) conventional TEG, (c) SEM image of the fabricated Si-NWs TEG, and (d) Influence of wires length on the maximum power P_{\max} , internal resistance R , and P_{calc} the expected power value from R (Watanabe et al., 2017).

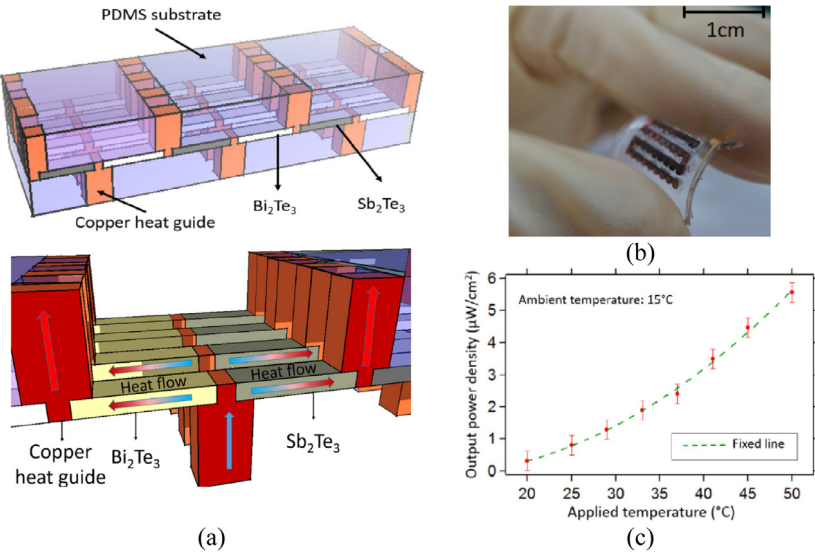


Fig. 10. Y-type flexible-TEG presented by Huu et al. (2018): (a) Schematic principle, (b) The fabricated device, and (c) Output power density.

wireless sensors to monitor aircraft security, flight tests, and safety (Dilhac et al., 2014). Because of the miniaturized form of wireless sensors nodes, the used thermocouples are limited in dimensions and require small temperature detection (heat source temperature lower than 100 °C). In a typical active mode, WSNs need 10 to 100 mW of power consumption and 10 to 50 μW at sleep mode.

Wang et al. (2013) presented experimental and numerical work of Bismuth Telluride (Bi₂Te₃)-based TEG for powering WSN

nodes for BEM applications. The authors investigated the matching of the generators' internal resistance with the power management module input system. Three TEGs configurations were presented: The first one consists of one single arrangement of 576 thermocouples with an internal resistance of 40 Ω. The TCs were fabricated on a 50 × 50 mm²-area including two ceramic plates (Fig. 11a). The second one was made of two parallel-connected 288 thermocouples with an internal resistance of 9.9 Ω. The last one consisted of three parallel-connected 192 thermocouples with an internal resistance of 4.1 Ω. Fig. 11b presents the impedance matching between the TEGs internal resistances

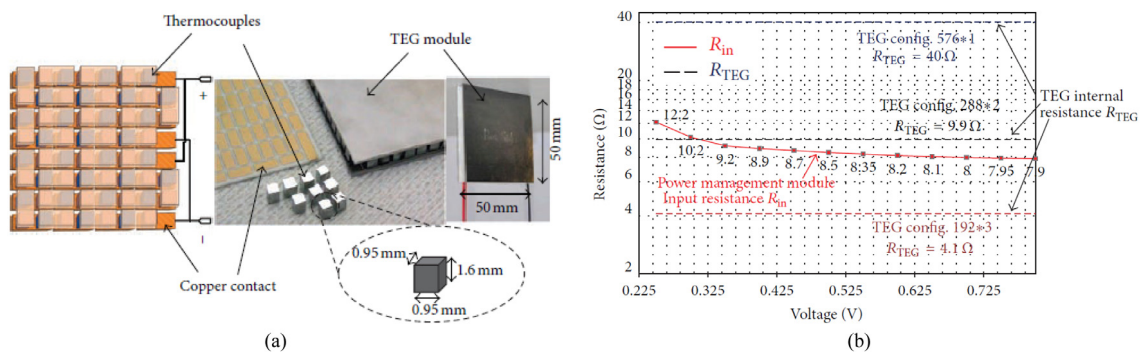


Fig. 11. (a) Vertical Bi_2Te_3 -based TEG for WSN applications (Wang et al., 2013), (b) Impedance matching investigation of the TEG internal resistance and the input resistance of the power management module (Wang et al., 2013).

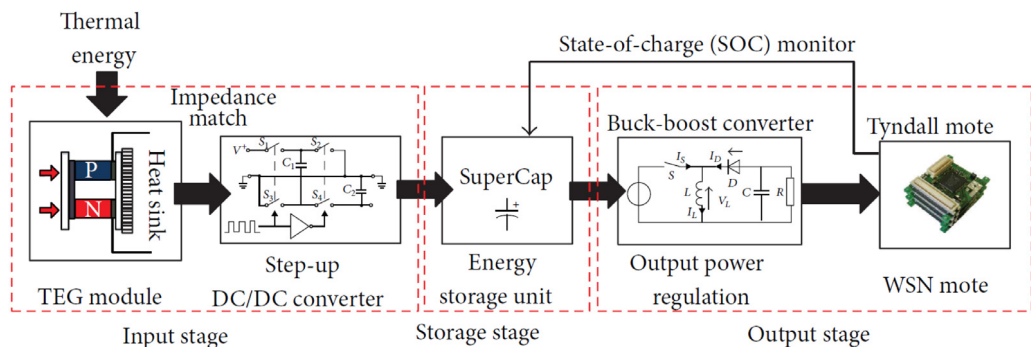


Fig. 12. TEG diagram for self-powered WSN-based applications (Wang et al., 2013).

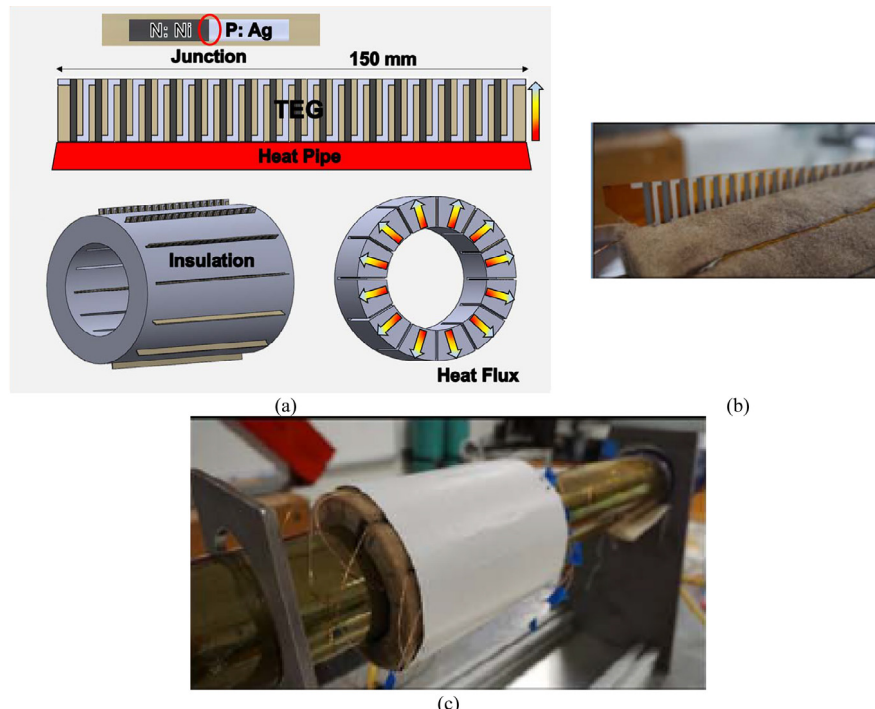


Fig. 13. Flexible TEG on heat pipe for WSN application (a) schematic illustration of the TCs and flexible TEG on pipe arrangement, (b) Module insertion, and (c) Complete device on pipe (Iezzi et al., 2017).

and the input resistance of the power management module. The convenient resistance to the input resistance of the power management module was corresponding to the second type of TEG with an error of less than 10%. The two parallel-connected 288 TCs present an output voltage of 280–450 mV at a temperature

difference of 3–5 °C. The wireless sensing module including the thermoelectric generator contains four main units to collect and transmit data: a DC/DC converter, energy storage unit (like Super-Capacitors), output power regulation and WSN mote acting like a

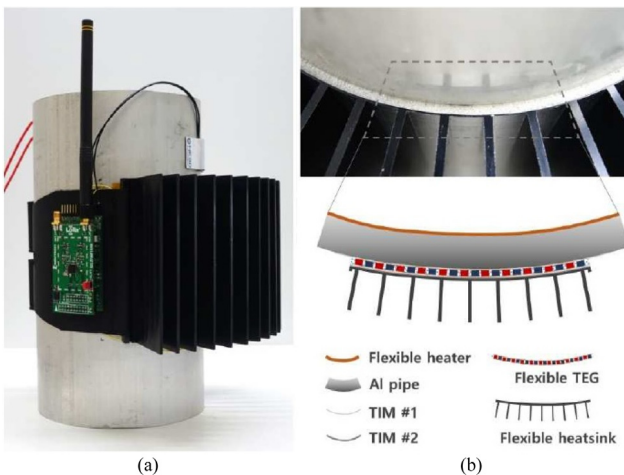


Fig. 14. Flexible TEG with a flexible heat sink located on a heat pipe for WSNs applications: (a) Side view of the f-TEG and shaped heat sink, (b) Top and schematic view of the f-TEG and heat sink with the two double-sided adhesive tapes (Kim et al., 2018).

receiver. Fig. 12 presents the TEG diagram for self-powered WSN cells.

Iezzi et al. (2017) presented a flexible planar TEG to extract heat from industrial heat pipes to self-powering a wireless sensor network. The proposed TEG was made with 420 Ag/Ni thermocouples screen printed on a flexible substrate to adapt to the cylindrical form of the pipe (Fig. 13). He used the same diagram given in Fig. 12 (Wang et al., 2013) to receive and transmit data to WSN nodes. The TEG produces an output power of 308 μW at a temperature difference of 127 °C.

Similarly, Kim et al. (2018) presented a flexible vertical TEG used for self-powering a WSN for industrial smart-buildings monitoring. The f-TEG was shaped and tested around an aluminum heat pipe with the integration of a flexible heat sink (Fig. 14a). To achieve such elasticity, authors fabricated a very thin aluminum-based heat sink to be suitable with the pipe shape. To avoid thermal resistance increasing, a graphite layer acting like a thermal interface material (TIM) was added between the TEG and the flexible heat sink. Also, in order to increase thermal emissivity, the heat sink surface was black-anodized with Al_2O_3 . Two double-sided adhesive tapes were added to electrically insulating the TEG with the heat pipe and the TEG with the graphite layer (Fig. 14b).

TEGs are a promising solution for supplying WSN nodes and to substitute the use of batteries, like lithium and alkaline, because of the extremely high maintenance cost of batteries (Tuna and Gungor, 2016; Liu and Wu, 2019). TEGs are capable to produce enough power to supply WSN nodes which typically consume average energy of 100 mWh (Penella et al., 2009). When assuming a small residential house contains 100 WSN nodes supported by lithium-ion batteries, the use of TEGs instead of batteries over 20 years will result in \$2000 savings (with a battery cost of \$5 and without including the maintenance cost). This economic cost is much higher in larger housing and industrial buildings.

3.3. In industrial electronic devices

Waste heat is a complex problem in many electronic devices such as central processing units (CPUs), integrated circuits, etc. CPUs produce thermal power in the range of 6–320 W, depending on the product's type, and generate a huge amount of wasted heat up to 110 °C. Table 3 resumes thermal and dimension properties for various CPU types (Intel, 2018). The waste heat emitted from the die during its operating could be turned into an advantage

by reusing this thermal energy to supply other components in the device or to activate the cooling fan, which will lead to an increasing battery's performance and lifetime.

In 1995, Suski (1995) invented an apparatus for recovering power from a semiconductor circuit using a thermoelectric generator. The generator was located between the integrated circuit and the heat sink whereas a fan was positioned above the heat sink to provide heat sink's cooling which results in reducing the temperature of the die. Fig. 15a illustrates the placement of the conventional components on a computer system (Ref. Glatz et al., 2009), which comprise an integrated circuit (Ref. Qing et al., 2018) installed on a motherboard (Ref. Leonov, 2013), an exhaust fan (Ref. Chen et al., 2018), a heat sink (Ref. Gongora-Rubio et al., 2001) and other components of a computer unit. As the inventor referred, the exhaust fan alone may not provide enough cooling. Eventually, adding another fan will solve the problem. Fig. 15b presents the invented structure, where a thermoelectric generator (Ref. Simon, 1961), or as it is mentioned in the paper "A Peltier cooler operating in the Seebeck mode", placed between a semiconductor device (Ref. Qing et al., 2018) (CPU), and a heat sink (Ref. Ge et al., 2018). The DC generated power from the generator will eventually supply the newly added fan (Ref. Crane and LaGrandeur, 2010) located on the top side of the heat sink. In fact, increasing the heat released by the integrated circuit leads an increase in the temperature difference between the hot and cold sides of the TEG which increases the generator's and fan's output powers. Eventually, the heat of the integrated circuit will be automatically controlled by the airflow from the fan.

Solbrekken et al. (2004) and Zhou et al. (2008) improved Suski's invention by using a "shunt attach" configuration. This latter consists of creating an alternative heat track to a shunt heat sink to enable sufficient electricity to be generated by the TE module to power-supply the cooling fan (Fig. 16a). Fig. 16b shows the experimental set-up when using TEG on the processor. Using TEG on shunt according to Zhou et al. showed an improvement in the delivered power compared to a conventional placement. Indeed, from a Pentium III working at 1 GHz, the used commercial TEG on shunt produced an electrical power of 6.7 mW compared to TEG on CPU (1.5 mW). In addition to powering cooling fans, TEGs were able to power-supply magneto-fluid-dynamic (MFD) pump to drive a liquid metal coolant in a computer chip (Ma and Liu, 2007). Fig. 17 presents the schematic diagram and prototype of the TEG mounted on the MFD channel. In this study, the authors used a commercial TEG (TEC1-127.08), with dimensions of 40 mm × 40 mm × 3.8 mm, located between a heat sink and a finned heat exchanger. The TEG was able to produce electrical power in the range of 10 mW to 100 mW to supply the MFD pump and to drive the metal liquid flow loop in order to cool the die.

Rosales et al. (2018) invented a TEG-based energy harvesting system for mobile phones. The invention serves to use the heat released by the electronic devices integrated inside the mobile phone like the camera, the display, the printed circuit board (PCB) and the die. The invention also consists of creating a new methodology that enables heat-losses decreasing from the heat sources to the TEG. This optimization is presented by adding two TEGs between a heat-generating device and a thermal interface material acting as an insulating layer, and consists of thermally prevent heat dissipation towards the other electronic components (Fig. 18). The TEGs are surrounded by two thermal conductive layers with high thermal conductivity. The TEG's materials have low thermal conductivity compared to the thermal conductive layers. This approach provides achieving high-temperature difference across the TEG. The first insulation layer helps to conduct heat from the heat dissipation device to the TEG while the second conductive layer helps to drive the heat

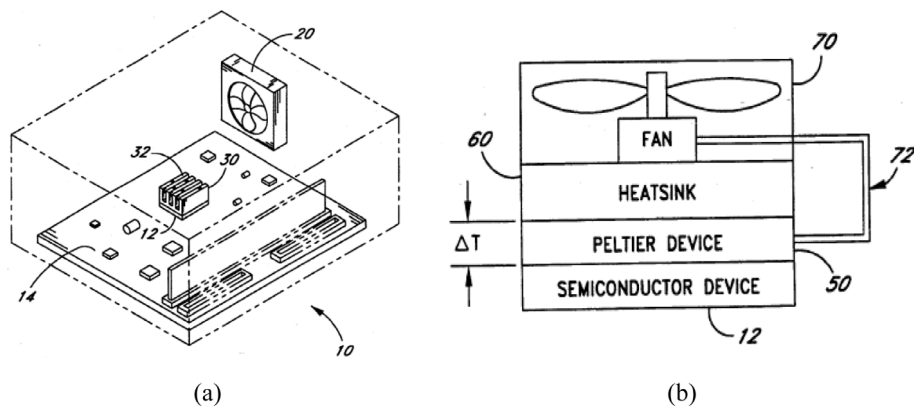


Fig. 15. Illustration of Suski's invention: (a) Conventional computer system with: die, conventional exhaust fan and heat sink. (b) The electrical connections between the TEG, fan and heat sink (Suski, 1995).

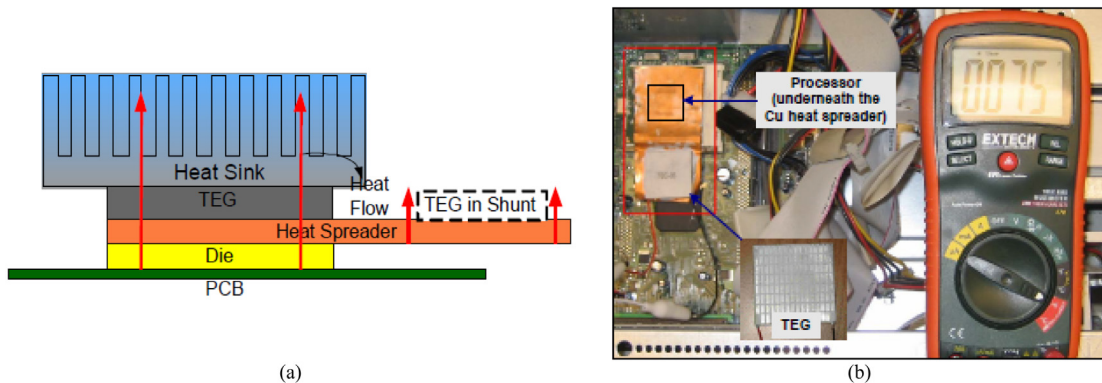


Fig. 16. Illustration of the TEG's placement: (a) TEG integrated on the CPU with shunt attach, (b) Experimental set-up of the used TEG on the processor (Zhou et al., 2008).

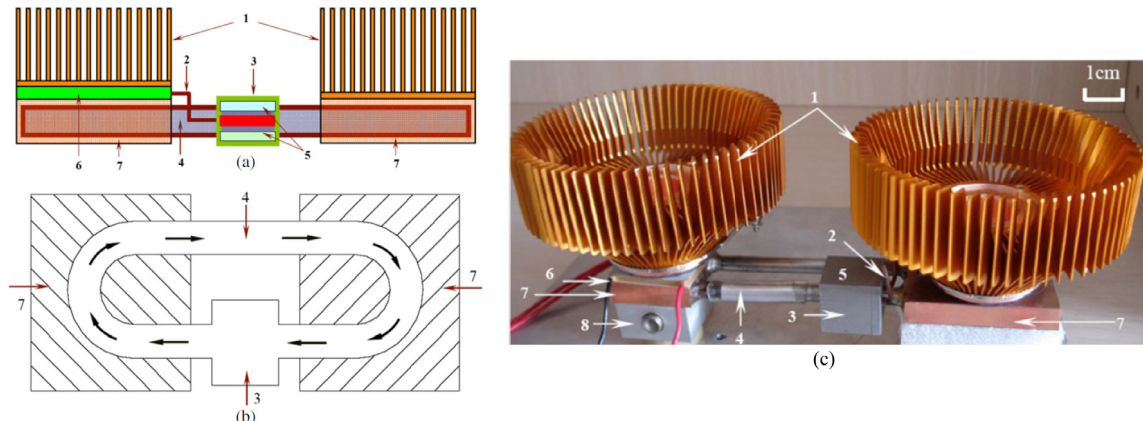


Fig. 17. MFD cooling pump driven by a commercial TEG with, finned heat exchanger (1), electrodes for TEG (2), MFD pump (3), liquid metal (4), magnetic plate (5), Thermoelectric generator (6), substrate (7), simulating chip (8): (a) Principle, (b) loop channel of the liquid coolant, and (c) prototype (Ma and Liu, 2007).

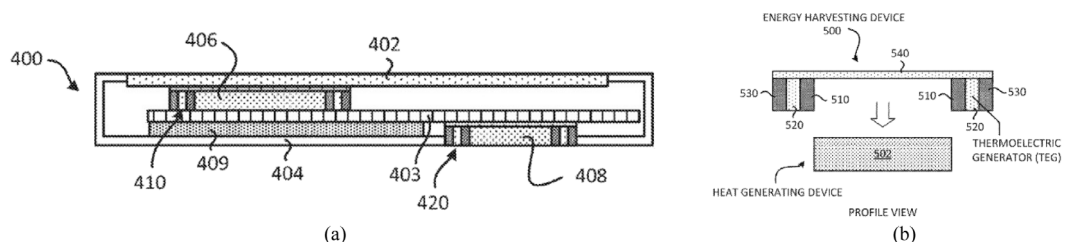


Fig. 18. Heat recovery system from mobile phone: (a) Illustration of profile view of the mobile device with, device (400), display (402), PCB (403), cover (404), Die (406), camera (408), battery (409), first energy harvesting device (410) and second energy harvesting device (420). (b) Illustration of the energy harvesting device (500) with, first thermal conductive layer (510), TEG (520), second thermal conductive layer (530) and an insulation layer (540) (Rosales et al., 2018).

Table 3
Intel's microprocessors properties (Intel, 2018).

CPU type	Package size (mm ²)		Thermal Design Power TDP (W)		T (°C)	
	Min	Max	Min	Max	Min	Max
Desktop	24 × 31	37.5 × 37.5	6	165	80	105
Mobile	12 × 12	42 × 24	2.2	57	80	105
Server	34 × 28	88 × 56.5	11.7	320	40	100
Embedded	25 × 27	45 × 42.5	3	105	40	110

from the TEG (Rosales et al., 2018). This methodology enables to harvest of about 1.5%-4.2% of the heat from the generating device.

Considering a maximum working thermal power of a desktop is 165 W and a conversion efficiency of TEG about 10%. Assume the desktop is working 24 h, 365 days a year, the converted electrical power by the TEG is: $16.5 \times 8760 / 1000 = 144.54$ kWh. The cost of electricity in the USA is 0.13 \$/kWh. Therefore, the cost economic by using the TEG for a year is: $0.13 \times 144.54 = \$18.78$. This cost economic is considered as 12.2% of the total electricity price of the mentioned desktop (with desktop's average power consumption is 135 W (Krzywaniak et al., 2018) and electricity cost of \$153.7 per year).

3.4. In automobile engines

Due to high fuel costs and carbon dioxide (CO₂) emission, many automotive industries are focusing on finding an alternative power source to reduce fuel energy costs and to improve engine performance. Industrialists are manifesting a big interest to thermoelectric generators (Espinosa et al., 2010; Crane and LaGrandeur, 2010; Orr et al., 2017; Cao et al., 2018; Mostafavi and Mahmoudi, 2018; Haidar and Ghojel, 2001; Yang, 2005; LaGrandeur et al., 2006), in order to convert the heat wasted by the exhaust gas, emitted from the internal combustion (IC) engine, into electrical energy. In a passenger vehicle, only 25% of the energy from fuel combustion is used for vehicle mobility and accessories running, while 40% is wasted as exhaust gas (Espinosa et al., 2010; Crane and LaGrandeur, 2010; LaGrandeur et al., 2006; Tang et al., 2015). In contrast, the amount of heat emitted from the exhaust system is very high and could vary from 100 °C to 800 °C with a thermal power up to 10 kW, depending on the vehicle speed and fuel category (Yang, 2005). This great amount of heat could be considered as a valuable source to generate sustainable and sufficient energy. Thus, converting the emitted heat will be the main solution to improve engine performance and supply additional electronic devices such as navigation systems, electronic braking, additional powertrain/body controllers, stability controls, telematics, and collision avoidance systems on conventional and hybrid vehicles. Also, this will reduce atmospheric pollution and power costs (Tang et al., 2015). Many international automotive industries are focusing on this field such as BMW (Crane and LaGrandeur, 2010; LaGrandeur et al., 2006), Ford (Hussain et al., 2009), Renault (Espinosa et al., 2010) and Honda (Mori et al., 2011). They have prototyped many TEGs for their new automobile generations.

Because of the high-temperature range in the internal combustion engine, using more than one type of thermoelements is required which will lead to better effective conversion efficiency. Segmented thermoelectric materials were often used in this kind of applications because of the large scale of extracted temperature. LaGrandeur et al. (2006) have arranged three stages segmented TE materials as follows: N- and P-type Bi₂Te₃ for low temperature range (< 250 °C), P-TAGS and N-PbTe for medium temperature range (250 °C–500 °C) and skutterudite materials (P-CeFe₃RuSb₁₂ and N-CoSb₃) for high temperature range (500 °C–700 °C). To control TE elements thicknesses, thermal expansion coefficient and to optimize the power efficiency of

the module, the authors develop a new TE arrangement for the segmented materials (Fig. 19). This new configuration utilizes a planar TC approach with segmented TE materials between the heat source and the heat sink (Fig. 19b). This approach supports the possibility of obtaining different areas, thicknesses and thermal expansion coefficients of the materials. In addition to the segmented TEGs, cascaded TEGs have also been presented for vehicle applications (Chen et al., 2017; Cheng et al., 2018; Krzywaniak et al., 2018). The independent mechanical arrangement in this approach allows avoiding the incompatibility problem of the segmented arrangement. Wilbrecht and Beitelshmidt (2018) presented two stages of cascaded TE materials for railway vehicles. The cascaded TEG was made of Bi₂Te₃ (220 °C) and Mg₂Si_{0.4}Sn_{0.6}/MnSi_{1.81} (410 °C) and produced electrical power of 2.5 kW.

Two TEG's locations were used in the literature in the IC engine: on the cooling system (radiator) and the exhaust heat exchanger. The first location was presented by Crane et al. (2001). They presented the modeling of a radiator integrated TEG and demonstrated its capability to extract enough power from the cooling system to supply the alternator function. Fig. 20a depicts the schematic that illustrates the TEG arrangement on the radiator. The generators were placed between the surface of the radiator and the fins. The maximum temperature difference between the radiator and the fins system was around 80 °C. Furthermore, the engine load affects the heat transfer to the radiator and then the TEG's output power. Fig. 20b presents the total radiator heat flow to the engine brake power and TEG output power versus the engine full power. The system with the use of Bi₂Te₃-based TEG and with low engine loads (25%) was able to generate an electrical power over 1 kW, which could self-supply the alternator and result in a significant fuel reduction improvement. However, experimental results about this approach have not been presented.

The second cited TEG's location is on the exhaust heat system. The heat exchanger allows transferring gaseous working fluid from the catalytic converter to the muffler (Fig. 21a). Heat exchangers are presented in two forms: flat and cylindrical forms. Placing the TEGs on the exhaust heat exchanger surface was the most cited placement from the literature because of the high generated temperature (Orr et al., 2017; LaGrandeur et al., 2006; Mori et al., 2011; Yu and Chau, 2009; Crane et al., 2013; Liu et al., 2016). The TE modules are connected in a matrix form to the exhaust system surface. The heat passing by the exhaust inlet to the exhaust outlet provides thermal energy to the TEGs hot sides. Fig. 21b presents the placement of 32 TEG modules, with 24 TCs each, on a flat exhaust gas (Mori et al., 2011). For the cold TE modules side, coolant heat exchangers, mostly liquid, are the most used to maintain the cold temperature (Mori et al., 2011). Orr et al. presented the use of gas heat exchangers with liquid heat pipes attached to both the cold and hot sides of the TEG (Orr et al., 2017). The hot gas comes from the exhaust heat and passes through exhaust channel where 8 water pipes are integrated into the channel fins and attached to the hot side of the 8 TEGs. A fan was placed in the cool air channel's inlet. The cold channel also presents 8 water heat pipes, integrated into the fins and attached to the cold side of the TEGs. Haidar and Ghojel utilized water-cooled heat sink to provide the minimum temperature at the cold

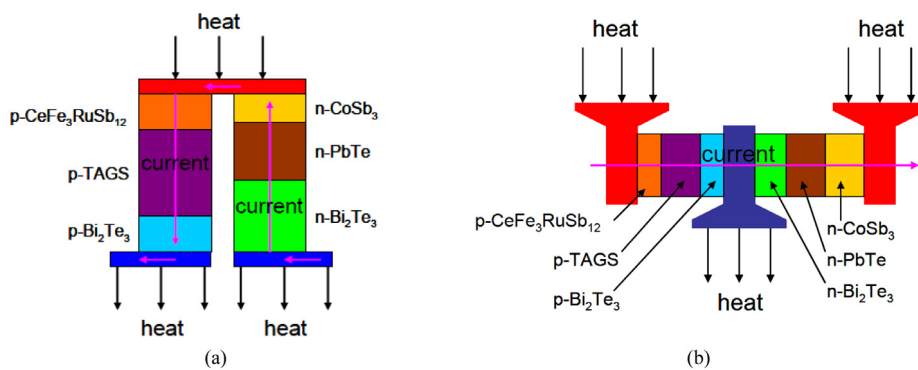


Fig. 19. (a) Conventional schematic of segmented material. (b) New TE couple configuration (Y shape) with segmented materials (LaGrandeur et al., 2006).

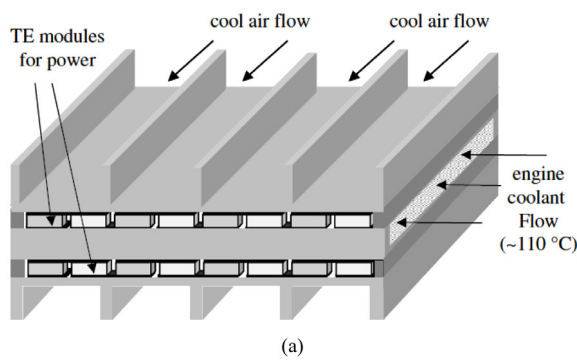


Fig. 20. TEG in radiator by Crane et al.: (a) Schematic illustration of the thermoelectric location in the radiator, and (b) The total radiator heat flow to the engine brake power and TEG output power versus percent of the engine full power (Crane et al., 2001).

junctions for 6 modules of 96 Bi₂Te₃-based TCs each and generate 14 W at $\Delta T = 200$ °C (Haidar and Ghojel, 2001). Hussain et al. (2009) presented a direct loop to the radiator with coolant fluid to maintain the cold junctions at lower temperatures.

Thermoelectric generator modules could be placed in different ways on the heat exchanger's surfaces: on the two (upper/lower) sides of the flat heat exchanger (Fig. 22a) (Mori et al., 2011; Yu and Chau, 2009; Quan et al., 2018), on the four surfaces of a flat heat exchanger (Fig. 22b) (Cao et al., 2018), and on all surfaces of a cylindrical heat exchanger which provides heat distribution in all possible directions (Fig. 22c) (Crane et al., 2012, 2013; Liu et al., 2016). Another TEG's placement approach on the exhaust system has been studied, to maintain high thermal energy, is placing the TE system inside the heat exchanger (Fig. 22d) (Hussain et al., 2009; Zhang et al., 2015; Risseh et al., 2018).

One of the encountered problems is the inhomogeneous temperature from the heat exchanger surfaces. This leads to an increase in the parasitic Peltier effect and a decrease in power efficiency. To avoid this mismatch temperature problem, thermally insulating TE modules or exhaust heat/coolant exchanger surfaces is needed (Mori et al., 2011). Tang et al. (2015) have proposed to insulate the hot sides of the TE modules using silica fiber of 0.1, 0.2 and 0.3 mm thicknesses. The proposed technique improved the output power with 22.5% compared to the TEG without thermal insulation. The output power increased from 14.12 W to 17.3 W at the same hot junction's temperature as the inlet temperature. This step also reduces the thermal conductivity and parasitic Peltier effect of the module and reduces power losses from 11% to 4.2%. Insulating the exhaust heat system has also been taken into consideration to decrease the temperature gap between the heat exchanger and TE modules.

In the previous studies, most of the researchers used commercial TEGs for the automotive sector. Gierth et al. (2018) allowed

the combination of ceramic and thick film-based technologies. They presented the fabrication of 3 thick-film thermocouples on ceramic-alumina (Al₂O₃) substrates (Fig. 23a). Fig. 23b shows the placement of the temperature sensor on the test rig. Two thermocouples types were fabricated and tested, Pt/PtRh10 and Ag/Pd, to investigate their long-term stability in harsh environments. The Pt/PtRh10 presents significant long-term stability at high temperatures and minimum aging issues compared to the Ag-Pd sensor for a temperature higher than 700 °C and air mass flow of 1000 L min⁻¹. According to these results, the authors have ameliorated the temperature sensor to a cylindrical form-TEG with 30 screen-printed TCs (Fig. 24). The experimental results of these sensors will be carried out in the future as the authors mentioned (Gierth et al., 2018).

The biggest financed and structured program for high-efficient thermoelectric waste heat recovery systems for passenger vehicles was developed by the Bell Solid-State Thermoelectric (BSST) team with the aid of the US Department of Energy for BMW vehicles and later for Ford vehicles. The project started from 2004 to 2012 with total funding of \$10,856,667 and passing by many development phases (Crane and LaGrandeur, 2011; Singh, 2007).

Table 4 presents the fabrication summary with different development phases for the thermoelectric exhaust heat recovery system developed by BSST for BMW and Ford Vehicles. The development phases started by the fabrication of fractional and full-scale low-temperature TEGs based on P- and N-type Bi₂Te₃ TE materials and passed by the integration of segmented TE elements, to handle the increased high temperature of the exhaust heat. Also, the phases carried the development of flat to cylindrical TEGs approaches to minimize thermal losses. Table 5 presents the advantages and disadvantages of each phase. Fig. 25 presents the different phases (from phase 1 (Fig. 25a) to phase 6 (Fig. 25f) respectively) for the development of vertical TEGs-based

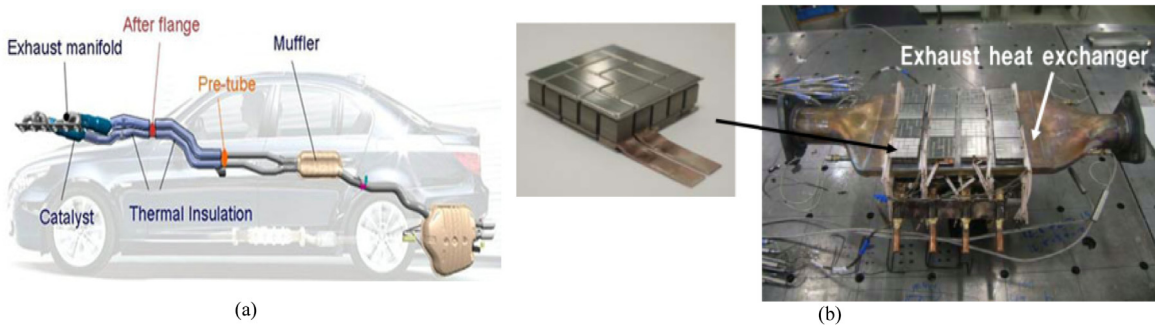


Fig. 21. Thermoelectric generator's positions: (a) Exhaust system inside a passenger vehicle (Crane and LaGrandeur, 2010). (b) TEG's assembly on a flat heat exchanger (Mori et al., 2011).

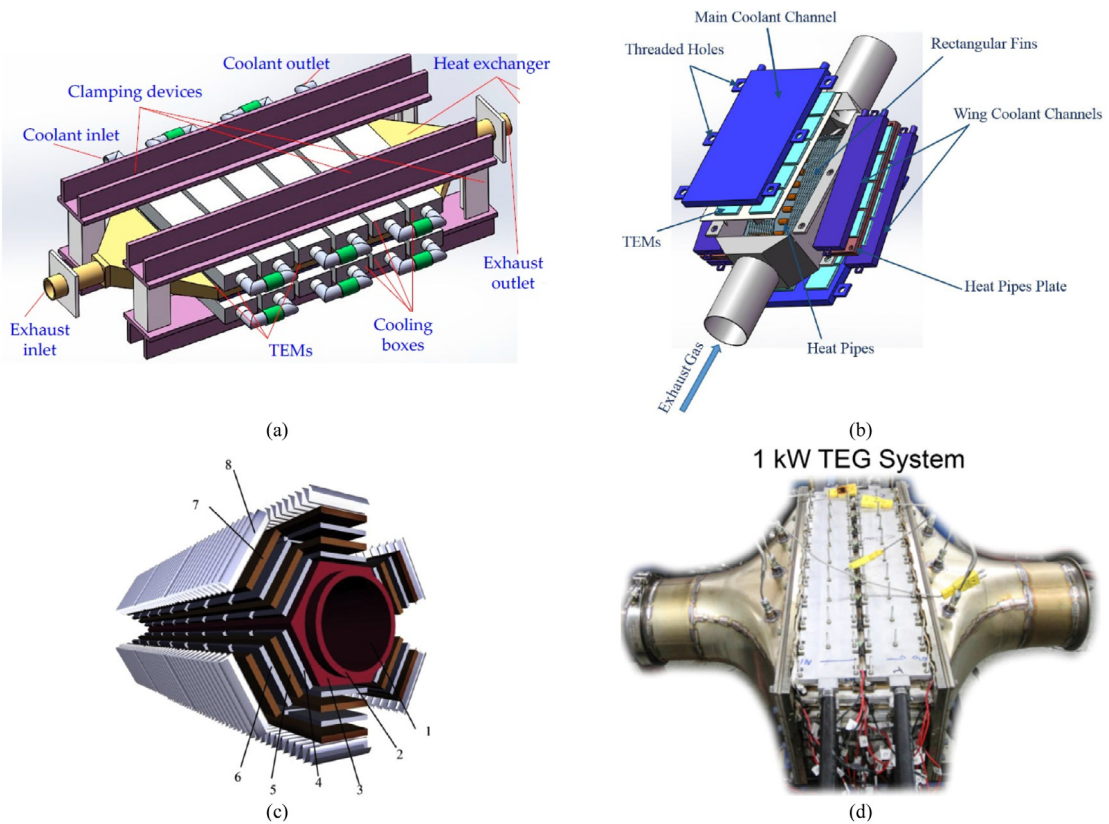


Fig. 22. Different thermoelectric exhaust heat systems: (a) TEG modules on the double sides of a flat heat exchanger (Quan et al., 2018), (b) TEG modules on the four sides of a flat heat exchanger (Cao et al., 2018) and (c) TEG modules on hexahedral (6 sides) heat exchanger with: Inner-side of the tube (1), main support tube (2), conducting oil (3), TEGs modules (4), aluminum plate (5), the second stage TEGs module (6), cooling plate (7), and fins (8) (Liu et al., 2016), (c) Nanobulk half-Heusler-based TEG system integrated into the exhaust heat system (Zhang et al., 2015).



Fig. 23. Ceramic-based thermocouples: (a) 3 Screen printed thermocouples and one reference PT100 platinum resistance thermometer on planar alumina substrates, (b) View inside the test rig with reference thermal sensor and thick-film validation sensor (Gierth et al., 2018).

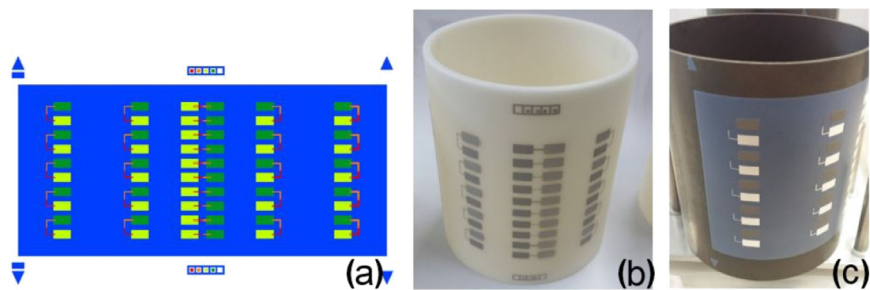


Fig. 24. Tubular screen-printing: (a) Layout of 30 TCs on a tubular surface, (b) Screen-printing on an alumina (Al_2O_3) substrate, and (c) Glass insulation paste on steel (Gierth et al., 2018).

exhaust heat recovery system for BMW and Ford vehicles by Crane et al. From the past studies, some points need to be taken into consideration for such an application in order to improve TEGs performance and fuel efficiency:

- Wisely choosing TE materials with a temperature range suitable with the high emitted heat from the engine (maximum of 700 °C);

- Placing the TEGs modules on the heat exchanger to convert high thermal energy;

- Decrease heat losses between the heat source and the module. Limiting the thermal gap and decrease the thermal contact resistance by thermally insulating the heat exchanger's surfaces or the TEGs surfaces and electrically isolate the surfaces between the TEG and the heating/cooling exchangers to decrease the parasitic electrical resistances;

- Considering the mechanical robustness of the TEGs against harsh environments and high pressure;

- Taking the vehicle speed into consideration: in fact, increasing the vehicle's speed will lead to exhaust temperature and mass flow increasing. However, this will damage the generator if the exhaust temperature is higher than the melting point temperature of the TE materials. Hence, to avoid these issues, we should decrease the exhaust backpressure and choose TE materials with a high melting point temperature.

Multiple efficiency factors are combined to analytically calculate the fuel cost saving (Liu et al., 2016): TEG's efficiency (η_{TEG}), the alternator efficiency (η_{ALT}) which is usually about 60%, the exhaust gases efficiency (η_{HX}) which is the ratio of the transferred gases from the fuel to the exhaust gases and is usually about 40%, engine thermal efficiency (η_{ENG}) which is about 30% and the efficiency of the heat exchanger which is usually between 40% and 70% (depends with the size and materials) and expressed as Haidar and Ghojel (2001):

$$\eta_{HEx} = \frac{T_{gas,in} - T_{gas,out}}{T_{gas,in} - T_{cool,in}} \quad (15)$$

For a 10% power efficiency of the TEG module and one-liter, diesel price is 0.794 \$/l, the fuel cost saving is:

$$\text{Fuel Cost Saving} = \frac{\eta_{TEG} \times \eta_{HX} \times \eta_{HEx}}{\eta_{ALT} \times \eta_{ENG}} \times \text{Fuel Cost} = 0.1588 \text{ \$/l} \quad (16)$$

The energy/fuel cost-saving efficiency is then 20% per one liter. The latest publications of TEG's based exhaust waste heat recovery systems are listed in Table 6.

3.5. In aerospace

TEGs, or RTGs for Radioisotope Thermoelectric Generators, are widely used in aerospace applications such as space crafts, satellites, and space probes. RTGs use the heat released by the natural decay of some radioactive materials to convert it into electricity. Consequently, the isotope materials determine the

characteristics of the RTG's heat source. Isotope used fuels should demonstrate many characteristics like low radiation emission, acceptable fuel half-life with the mission duration, high melting point, high-power density and being safe in all conditions. Five isotope materials with the required characteristics were developed for a long time by the Department Of Energy (DOE) and the US space missions: Cerium-144 (Ce-144), Polonium-210 (Po-210), Strontium-90 (Sr-90), Promethium-147 (Pm-147) and Plutonium-238 (Pu-238) (Streb, 1966). Table 7 presents the characteristics of isotope fuels. However, Ce-144, Po-210, Sr-90, and Pm-147 demonstrate many disadvantages while testing. Ce-144 provides half-life of 285 days and preferred to only work for 6 months space mission. It was developed to work in the orbit with the SNAP-1 power system (SNAP for System for Nuclear Auxiliary Power). Eventually, the power system results in high emission of beta/gamma radiation and failed in reentry tests from the orbit. Po-210 was first developed for the SNAP-3 by 1959. It presents the lowest radiation emission and requires low shielding. However, the power system presents very short half-life (138 days) for working on space missions. Sr-90 provides high working half-life (28 years) but it results in a very high radiation emission which requires heavy shielding to prevent the radiation. Pm-147 presents a high half-life of 2.6 years. It also presents low beta emission but very high gamma radiation.

Eventually, the most suitable isotope fuel is the high-cost Pu-238. It presents a high melting point, low gamma radiation and high half-life of 89.6 years which enables the use in long term missions without the need for a power-fluttering device. The features of this fuel enabled the launching of the first navigation satellite (Transit 4A spacecraft) fueled by the radioisotope power system SNAP-3 RTG by June 1961. Since then, the DOE and the US space missions have been focusing on producing the Pu-238 to use it for space programs (Streb, 1966). After that, NASA launched 47 RTGs for 27 space mission and earth orbit exploration for the Transit, Snapshot, Nimbus and Apollo missions.

In 1989, NASA launched the first modular GPHS-RTG (GPHS for General Purpose Heat Source) on Galileo spacecraft (Bennett et al., 1989). One GPHS-RTG module, fueled by Pu-238, provides 285 W of thermal energy at the beginning of the mission. Fig. 26a presents the overall structure of the GPHS-RTG. The cylindrical envelope of the RTG presents 0.42 m diameter and 1.14 m length and weighs of 55.9 kg. It contains 18 thermally coupled GPHS modules surrounded by 572 Silicon Germanium (SiGe) thermocouples with $2.74 \times 6.50 \text{ mm}^2$ cross-section for each N and P leg. Fig. 26b presents the structure of the SiGe thermocouple. The hot junctions of the TCs were made of Silicon Molybdenum (SiMo) and operate at 1308 K. The cold junctions operate at 566 K. The GPHS-RTG provides electric power of 245 W at 28–30 V DC (Bennett et al., 1989) and conversion efficiency of 6.5% to 7% (O'Brien et al., 2008).

The next generation of the RTG used in space missions is the Multi-Mission Radioisotope Thermoelectric Generator (MMRTG).

Table 4

Summary of the fabrication phases for the thermoelectric exhaust heat recovery system developed by BSST for BMW and Ford Vehicles.

Phases	Type of thermoelements	Number of TCs	Heat source	Cold side	Generated power [W]	Reference
Phase 1 (2006)	Fractional LT-TEG: p and n-types Bi ₂ Te ₃	2160 TCs (60 TEG modules)	PHx (fluid): 200 °C	Coolant pump (water): -5 °C	130	LaGrandeur et al. (2006) and Crane et al. (2009b)
	Full-scale LT-TEG: p and n-types Bi ₂ Te ₃	10800 TCs (300 TEG modules)	5 PHx (fluid): 210 °C	6 coolant pumps (water): 2.5 °C	500	
Phase 2 (2007)	Fractional MT-TEG: p-TAGS and n-PbTe	4TCs	Oil heat exchanger: 472 °C	Liquid heat exchanger: 33 °C	20	Crane et al. (2009a)
	Fractional-MT-TEG: - LT: p and n-Bi ₂ Te ₃ - MT: p-TAGS and n-PbTe	6TCs	Oil heat exchanger: 500 °C	Liquid heat exchanger: 20 °C	-	
Phase 3 (2008)	Segmented HT flatTEG: - LT: p and n-Bi ₂ Te ₃ - MT and HT: half-Heusler alloy (Zr, Hf)	-	Electric cartridge heater: 600 °C	Liquid cold plate: 25 °C	125	Crane and LaGrandeur (2010)
Phase 4 (2011)	LT cylindrical TEG: p and n-Bi ₂ Te ₃	-	Gaz heat exchanger: 435 °C	Liquid heat exchanger: 20°	205	Crane et al. (2012)
	MT-Segmented cylindrical TEG: - LT: p and n-Bi ₂ Te ₃ - MT: half-Heusler alloy (Zr, Hf)	-	Gaz heat exchanger: 620 °C	Liquid heat exchanger: 20 °C	608	
Phase 5 (2012)	MT-Segmented cylindrical TEG: - LT: p and n-Bi ₂ Te ₃ - MT: half-Heusler alloy (Zr, Hf)	-	-	-	- 712 (in test bench) - 600 (in real vehicle)	Crane et al. (2013)

Table 5

Advantages and disadvantages of the different phases of the thermoelectric exhaust heat recovery systems developed by BSST for BMW and Ford Vehicles.

Phases	Advantages	Disadvantages
Phase 1 (High-density Bi ₂ Te ₃ -based Flat TEG) (Crane et al., 2009b)	- High power density. - A power control system (PCS) reaches 99% DC-DC converter's efficiency for the fractional Bi ₂ Te ₃ TEG.	- Low-temperature range.
Phase 2 (Low-density Bi ₂ Te ₃ , P-TAGS and N-PbTe-based Flat TEG) (Crane et al., 2009a)	- Power efficiency 10%.	- Medium temperature range. - Low power density. - Low integration density.
Phase 3 (Half-Heusler alloy and Bi ₂ Te ₃ -based Flat TEG) (Crane and LaGrandeur, 2010).	- High-temperature range. - High power density.	- Mismatch of thermal interfacial resistance between the TEG and hot/cold heat exchangers.
Phase 4 (Half-Heusler alloy and Bi ₂ Te ₃ -based Cylindrical TEG) (Crane et al., 2012)	- Solving the problem related to the thermal expansion's inference found in phase 3.	- Medium-temperature range.
Phase 5 (Half-Heusler alloy and Bi ₂ Te ₃ -based Cylindrical TEG) (Crane et al., 2013).	- Improving the ring's diameter (from 1.5 mm to 0.05 mm) to achieve lower interfacial resistance between the hot side heat exchanger and the hot shunt interfaces. - Validation of the steady-state and transient conditions. - Testing on a real engine dynamometer for BMW X6 and on Lincoln MKT. - Adding an auxiliary water pump.	- Heat loss between the TEG and the environment because of the bypass valve. - The integrated system's weight and volume.

It was first developed in June 2003 and planned to work on planetary bodies like Mars and in the vacuum of space (Ritz and Peterson, 2004). The MMRTG was designed to operate for 14 years and to generate power of 110 W (minimum) at 28 V DC. The MMRTG (Fig. 27a) presents 8 GPHS modules fueled by Pu-238. It is made of 16 PbTe/TAGS modules and 48 TCs each connected electrically in series and located under the heat radiations fins (Fig. 27b). The RTG design was similar to that used for SNAP-19 for the Pioneer-10 and Viking missions. Moreover, the MMRTG-based design was developed to reduce the thermoelectric degradation found in previous studies. The study was focusing on reducing the P and N legs diameter (5.9 mm and 4.67 mm respectively for the N and P legs compared to 9.575 mm and 6.858 mm respectively for the N and P legs for the Pioneer

couple). Also, the MMRTG uses PbSnTe as hot side connection material and increasing the TAGS-base P leg hot side's temperature to 121.11 °C by increasing the P leg thickness. The MMRTG was capable to operate at 510 °C hot temperature (compared to 371 °C for the Pioneer and Viking-based RTGs) (Hammel et al., 2009). The MMRTG is addressed to work for MSL and Mars missions by 2020 (Holgate et al., 2015).

To increase the performance of RTGs in terms of materials, design, and efficiency, Holgate et al. presented an enhanced MMRTG (Holgate et al., 2015). The proposed design was made of 768 skutterudite (SKD)-based TCs with nickel-based connectors. The SKD-based eMMRTG, for Enhanced Multi-Mission Radioisotope Thermoelectric Generator, was able to operate under 600–625 °C hot temperature and 100–200 °C cold temperature. The eMMRTG

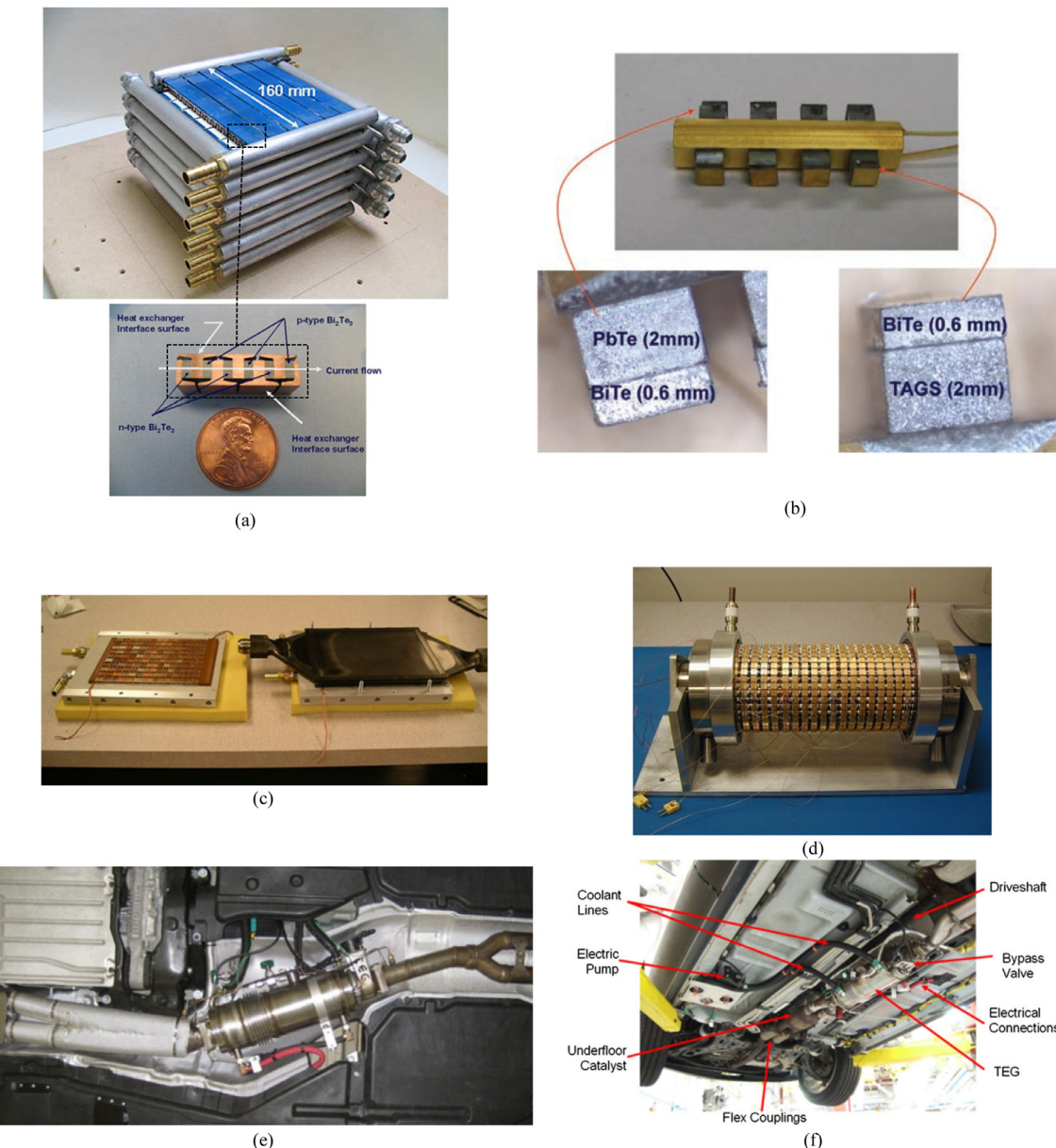


Fig. 25. Different phases for the development of vertical TEGs-based exhaust heat recovery system for BMW and Ford vehicles by Crane et al.: (a) Phase 1: Full-scale Bi₂Te₃ with 5 heat exchangers and 6 coolants (500 W at $\Delta T = 207^\circ\text{C}$) (Crane et al., 2009b), (b) Phase 2: 10% Efficient Pb/TAGS/BiTe Fractional TGM Hot Subassembly (Crane et al., 2009a), (c) Phase 3: Single-layer high-temperature segmented TEG (Crane and LaGrandeur, 2010), (d) Phase 4: Bi₂Te₃ cylindrical TEG device, (Crane et al., 2012), (e) Phase 5: TEG integration into the exhaust line of the BMW X6 prototype vehicle (Crane et al., 2013), (f) Phase 6: Integration of the TEG into the underfloor of the Ford Lincoln MKT vehicle (Crane et al., 2013).

generates electrical power of 90–105 W at the beginning of life and conversion efficiency of 7.6–8.3% compared to 6% for the PbTe/TAGS MMRTG (Holgate et al., 2015).

Also, to satisfy the demand of power-supplying the low-power devices in the space systems, many researchers focused on developing low-power radioactive thermoelectric generators. Liu et al. (2017) developed a micro-radial milliwatt-power RTG. The fabricated RTG was made of four TE modules and a radioisotope heat source covered by an aluminum cylinder box. Fig. 28 presents the micro-radial milliwatt-power RTG's experimental prototype (Fig. 28a) and the simulated structures respectively with 4, 6 and 8 modules (Fig. 28b-d). An electric heating aluminum oxide-based helm with an internal resistance of $3.2\ \Omega$ was used in the simulations to perform as an Am-241 isotope heat source. The heat source with a dimension of $7 \times 7 \times 27\ \text{mm}^3$ was wrapped by a copper-based shielding. The thermocouples were made of

low-temperature Bi₂Te₃ with P and N legs with dimensions of $10 \times 3 \times 1\ \text{mm}^3$. The fabricated RTG presents an output voltage of 92.72 mV and electrical power of $149\ \mu\text{W}$ at 0.1 W heat source's power.

Liu et al. (2018b) have developed an RTG based on concentric filament architecture for low power aerospace microelectronic devices. The RTG was made of 16 filaments, fabricated using simple brush coating (Fig. 29a). Two structures were fabricated: arrayed structures (Fig. 29b) and cylindrical ones (Fig. 29c). The arrayed RTG was able to produce an electrical voltage of 83.5 mV and an electrical power of $32.1\ \mu\text{W}$ with a planar heat source and temperature of 398.15 K. The cylindrical RTG produces 156.7 mV of electrical voltage and $85.8\ \mu\text{W}$ of electrical power with a cylindrical at the same heat source temperature.

Yuan et al. presented a radial micro screen-printed planar RTG for lightweight applications in space missions (Yuan et al.,

Table 6

Publications summary of TECS' based exhaust waste heat recovery system in automobiles.

Authors	Size	Number of TECS	Type of TCs	Generated power	Type of tested vehicle/engine	Conversion efficiency	Fuel consumption	Type of study
Espinosa et al. (2010)	SWS: ^a 50 × 31 × 10 (cm ³)	-	– Low temperature: Bi ₂ Te ₃ /(BiSb) ₂ Te ₃ , – High temperature: Mg ₂ Si/Zn ₄ Sb ₃	1200 W	Renault	–	–	– Simulation
								– Experimental
Mori et al. (2011)	SWS: 3600 cm ³	32	Low, Medium and High-temperature TE modules	225 W Th ≈ 500 °C ΔT ≈ 330 °C	Honda 1.3L Civic	–	3%	– Simulation
								– Experimental
Jeng and Tzeng (2013)	SOT: ^b 40 × 40 (mm ²)	6	–	16 W	Toyota 2200 c.c.	–	–	Experimental
Zhang et al. (2015)	SWS: 513 × 232 × 190 (mm ³)	400	Nanobulk half-Heusler alloy	1 kW Th ≈ 550 °C ΔT ≈ 339 °C	–	2.1%	–	– Simulation
								– Experimental
Temizer and İlkiç (2016)	SOT: 5.6 × 5.6 × 5 mm ³	40	–	156.7 W Th ≈ 250 °C Tc = 100 °C	Diesel P8602 Fiat Doblo	–	–	– Simulation
								– Experimental
Orr et al. (2017)	SOT: 68 × 68 (mm ²)	8	–	38 W Th = 250 °C Tc = 54 °C	3.0 L V6 engine.	2.46%	1.57%	Experimental
Liu et al. (2016)	SWS: 450 × 350 × 15 (mm ³) SOT: 40 × 40 × 4.2 (mm ³)	96	Bi ₂ Te ₃	250 W at Th = 746 °C	–	5.35%	–	– Theoretical
								– Experimental
Quan et al. (2018)	SWS: 1420 × 670 × 185 (mm ³) SOT: 56 × 56 × 6 (mm ³)	240	Bi ₂ Te ₃	608.85 W at Th = 247 °C Tc = 75 °C	Military SUV with four-cylinder diesel engine	1.03%	–	Experimental
Cao et al. (2018)	SOT: 40 × 40 × 4 (mm ³)	36	Bi ₂ Te ₃	13.08 W at Th = 300 °C	–	2.58%	–	Experimental

^aSWS: Size of Whole Structure.^bSOT: Size of One TEG.**Table 7**

Characteristics of isotope materials for space missions (Streb, 1966).

Isotope	Isotope fuel form	Watts cm ⁻³	Half-life	Melting point (°C)	Weight density (g/cm ³)	Specific activity (W/Kc)	Decay particle
Po-210	Metal	1210	138 d	254	9.3	31.7	Alpha
Pm-147	Pm ₂ O ₃	1.5	2.6 y	2300	5.55	0.37	Beta
Sr-90	SrO ₂	0.93	28 y	2430	2.65	6.5	Beta
Pu-238	PuO ₂	5.0	89.6 y	2250	11.46	34.5	Alpha
Ce-144	CeO ₂	13.8	285 d	2680	7	7.9	Beta

2018). The proposed RTG was made of N-type Bi₂Te_{2.7}Se_{0.3}, P-type Bi_{0.5}Sb_{1.5}Te₃, and P-type Sb₂Te₃ and screen-printed on a polyimide substrate (Fig. 30). The fabricated RTG was able to generate 6.31 μW at 35.66 mV when the PuO₂-238 radioactive heat source produces 1.564 W thermal energy.

However, the cost production and deployment of RTGs are very high because of the needed safety protection of the nuclear materials and because of the high cost and low disposal of Pu-238, where a gram of Pu-238 costs \$1,968 (Werner et al., 2016). The cost production of an RTG reached \$118M for GPHS-RTG and \$109M for MMRTG. However, the important need of Plutonium-238 as fueling, despite its very high production cost, is an important limitation for RTGs production which leads to an emergent necessity in improving the efficiency of the radioisotope power system (RPS) (Hayhurst et al., 2019; R.P.S. Committee, 2009).

In order to minimize the use of Pu-238 and to increase the efficiency of RPS, NASA started developing a dynamic thermoelectric

conversion system: ASRG (Advanced Stirling Radioisotope Generator) (Mason, 2007; Qualls et al., 2017). This dynamic converter uses a Stirling engine and produces a conversion efficiency of up to 30% while using half of the thermal energy as the RTG. However, using converters with moving mechanical parts will always be exposed to maintenance problems. Furthermore, the research should focus on combining these two designs technologies while they are using the same heat source (GPHS), in order to produce higher electrical power for space applications and without the need of increasing the number of GPHS (i.e. same as Pu-238) in order to increase the electrical power in a single machine.

4. Conclusion

In this paper, we presented an in-depth analysis of thermoelectric generators for the recovery of waste thermal energy in

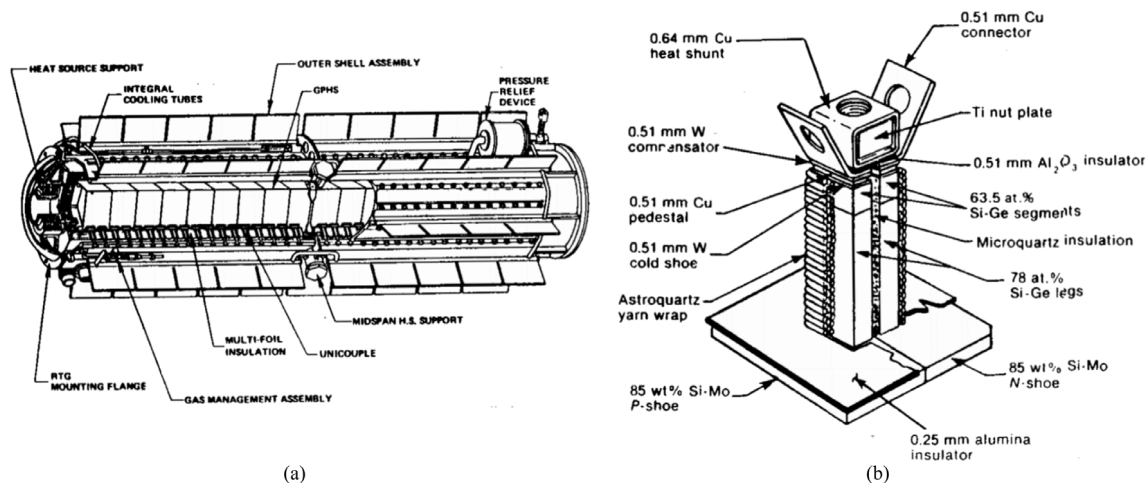


Fig. 26. The General-Purpose Heat Source Radioisotope Thermoelectric generator (GPHS-RTG), (a) overall structure, (b) SiGe thermocouple (Bennett et al., 1989).

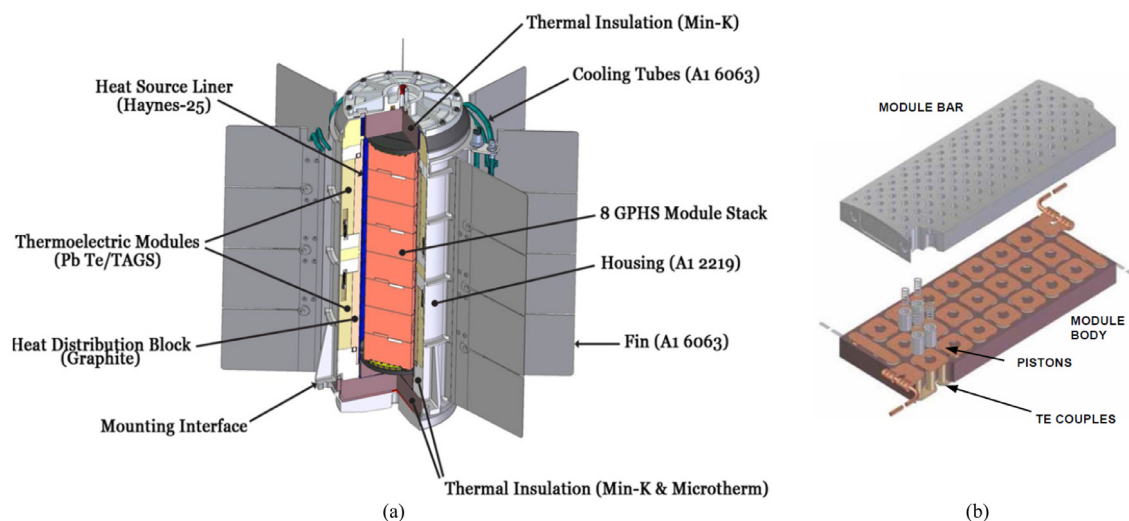


Fig. 27. Multi-mission radioisotope thermoelectric generator (MMRTG): (a) MMRTG cutaway, (b) TE module (Hammel et al., 2009).

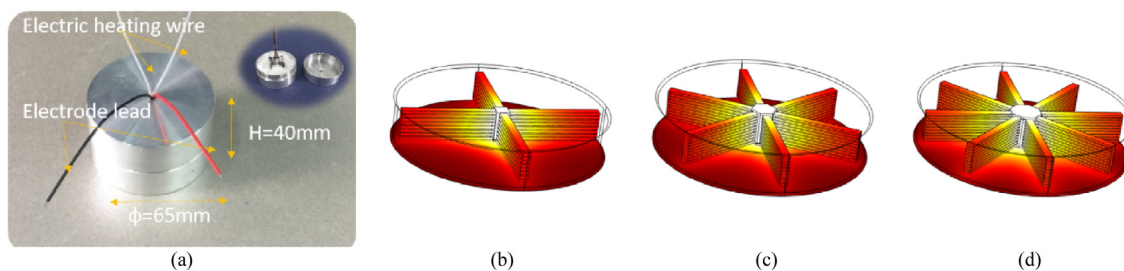


Fig. 28. A micro-radial milliwatt-power RTG: (a) Experimental prototype, (b) RTG with 4 modules, (c) RTG with 6 modules, and (d) RTG with 8 modules (Liu et al., 2017).

various sectors using the latest advanced thermoelectric generators designs, materials, and technologies. Thermoelectric generators have proved their usefulness in low and even high-power devices, as well as miniaturized and bulk applications depending on the generated power range, materials, and manufacturing process. Many applications were introduced, as well as their energy sources and cost economic ratio, like wireless sensor networks (WSNs), wearable and implantable devices (IoT and medical applications), industrial electronic devices, automobiles, and aerospace applications. Furthermore, according to Research

and Markets, the market size of thermoelectric generators is expected to rise from US\$460M in 2019 to US\$741M by 2025 (with an 8.3% compound annual growth rate) (Markets, 2019). With more than 500 scientific papers published every year, the automotive sector is subjected to lead the TEGs market as well as R&D for thin film based TEGs. One of the encountered issues in the mentioned studies is the parasitic thermal resistances generated from thermal heat losses, especially for high-temperature range applications, which decreases significantly the performance of the conversion efficiency. Also, researchers are trying to improve the conversion efficiency, using new technologies, miniaturization,

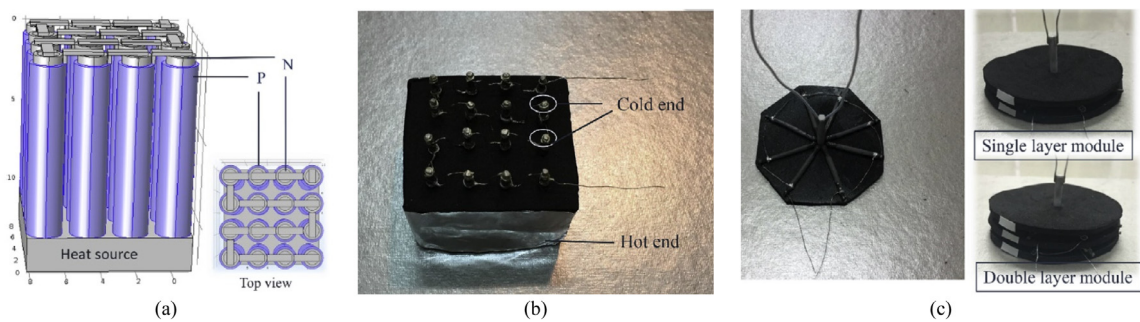


Fig. 29. Filament-based vertical/vertical RTG: (a) Concentric filament structure, (b) Arrayed filament-based RTG, and (c) Cylindrical filament-based RTG (Liu et al., 2018b).

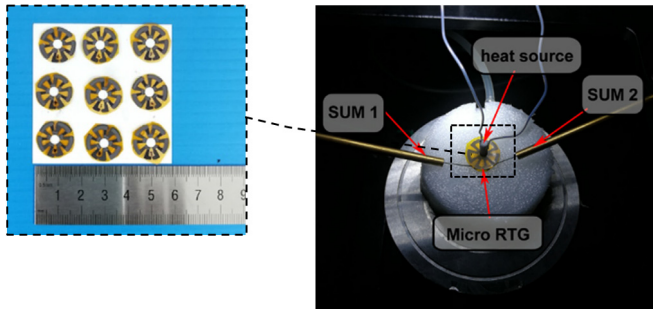


Fig. 30. Thick film planar RTG (Yuan et al., 2018).

increasing the number of thermocouples, limiting the parasitic resistances, etc. but they ignore the need of optimization in term of design of the TE modules and TC legs to have lower internal resistance in order to provide higher electrical power of such devices without the need of utilizing new TE materials with high power factor or increasing the number of TCs. In fact, the electrical internal resistance of the TEG modules plays the main role in order to provide higher electrical power which also depends in the first place on the TCs and connectors dimensions.

Declaration of competing interest

The authors declare that they have no known competing financial interests or personal relationships that could have appeared to influence the work reported in this paper.

Funding

The first author would like to thank the German academic exchange service (DAAD) organization, Germany, for providing financial support. The authors acknowledge the support for the Article Processing Charge by the German Research Foundation (DFG) and the Open Access Publication Fund of the Technische Universität Ilmenau.

References

- Amar, A.B., Kouki, A., Cao, H., 2015. Power approaches for implantable medical devices. *Sensors* 15, 28889–28914.
- Aravind, B., Raghura, G., Kishore, V.R., Kumar, S., 2018. Compact design of planar stepped micro combustor for portable thermoelectric power generation. *Energy Convers. Manage.* 156, 224–234.
- Bavel, M.V., Leonov, V., Yazicioglu, R., Torfs, T., Hoof, C.V., Posthuma, N.E., Vullers, R., 2008. Wearable battery-free wireless 2-channel EEG systems powered by energy scavengers. *Sensors Transducers J.* 94 (7), 103–115.
- Beltrán-Pitarch, B., Prado-Gonjal, J., Powell, A., Ziolkowski, P., García-Cañadas, J., 2018. Thermal conductivity, electrical resistivity, and dimensionless figure of merit (ZT) determination of thermoelectric materials by impedance spectroscopy up to 250 °C. *J. Appl. Phys.* 124, 1–7.
- Bennett, G.L., Whitmore, C.W., Amos, W.R., 1989. On the development of the power sources for ULYSSES and GALILEO missions. In: Proceedings of the European Space Power Conference, Madrid, Spain.
- Boukai, A., 2017. Matrixindustries. [Online]. Available: <https://www.matrixindustries.com/en/news/worlds-first-smartwatch-that-never-needs-charging>. [Accessed 2019].
- Brewster, S., 2016. Technologyreview. [Online]. Available: <https://www.technologyreview.com/s/602874/body-heat-powers-this-smart-watch/>. [Accessed 2019].
- Cao, Q., Luan, W., Wang, T., 2018. Performance enhancement of heat pipes assisted thermoelectric generator for automobile exhaust heat recovery. *Appl. Therm. Eng.* 130, 1472–1479.
- Chen, Y.-W., Wu, C.-C., Hsu, C.-C., Dai, C.-L., 2018. Fabrication and testing of thermoelectric CMOS-MEMS microgenerators with CNCs film. *Appl. Sci.* 8 (7), 1047–1059.
- Chen, T., Zhuge, W., Zhang, Y., Zhang, L., 2017. A novel cascade organic Rankine cycle (ORC) system for waste heat recovery of truck diesel engines. *Energy Convers. Manage.* 138, 210–223.
- Cheng, K., Qin, J., Jiang, Y., Lv, C., Zhang, W.B.S., 2018. Performance assessment of multi-stage thermoelectric generators on hypersonic vehicles at a large temperature difference. *Appl. Therm. Eng.* 130, 1598–1609.
- Crane, D., Jackson, G., Holloway, D., 2001. Towards optimization of automotive waste heat recovery using thermoelectrics. *SAE Tech. Paper* 1 (1021).
- Crane, D., Korpella, C., Jovovic, V., 2012. Validating steady-state and transient modeling tools for high-power-density thermoelectric generators. *J. Electron. Mater.* 41 (6), 1524–1534.
- Crane, D., Kossakowski, D., Bell, L., 2009a. Modeling the building blocks of a 10% efficient segmented thermoelectric power generator. *J. Electron. Mater.* 38 (7), 1382–1386.
- Crane, D., LaGrandeur, J., 2010. Progress report on BSST-Led US department of energy automotive waste heat recovery program. *J. Electron. Mater.* 39 (9), 2142–2148.
- Crane, D., LaGrandeur, J., 2011. Automotive waste heat conversion to power program-2011 vehicle technologies program annual merit review. In: DOE OVT Review.
- Crane, D., LaGrandeur, J., Harris, F., Bell, L., 2009b. Performance results of a high-power-density thermoelectric generator: Beyond the couple. *J. Electron. Mater.* 38 (7), 1375–1381.
- Crane, D., LaGrandeur, J., Jovovic, V., Ranalli, M., Adldinger, M., Poliquin, E., Dean, J., Kossakowski, D., Mazar, B., Maranville, C., 2013. TEG on-vehicle performance and model validation and what it means for further TEG development. *J. Electron. Mater.* 42 (7), 1582–1591.
- Dilhac, J., Monthéard, R., Bafleur, M., Boitier, V., Durand-Estèbe, P., Tounsi, P., 2014. Implementation of thermoelectric generators in airliners for powering battery-free wireless sensor networks. *J. Electron. Mater.* 43 (6), 2444–2451.
- Elmoughni, H., Menon, A., Wolfe, R., Yee, S., 2019. A textile-integrated polymer thermoelectric generator for body heat harvesting. *Adv. Mater. Technol.* 1800708, (1 of 6).
- Espinosa, N., Lazarid, M., Aixala, L., Scherrer, H., 2010. Modeling a thermoelectric generator applied to diesel automotive heat recovery. *J. Electron. Mater.* 39 (9), 1446–1455.
- Ge, Y., Liu, Z., Sun, H., Liu, W., 2018. Optimal design of a segmented thermoelectric generator based on three-dimensional numerical simulation and multi-objective genetic algorithm. *Energy* 147, 1060–1069.
- Gierczak, M., Prażmowska-Czajka, J., Dziedzic, A., 2017. Design, fabrication and experimental characterization of mixed thick-/thin film thermoelectric microgenerators based on constantan/silver. In: 21st European Microelectronics and Packaging Conference (EMPC) & Exhibition, Warsaw, Poland.
- Gierczak, M., Prażmowska-Czajka, J., Dziedzic, A., 2018. Thermoelectric mixed thick-/thin film microgenerators based on constantan/silver. *Materials* 11 (1), 1–9.

- Gierth, P., Rebenkau, L., Augsburg, K., Bachmann, E., Niedermeyer, L., 2018. Novel thermocouples for automotive applications. *J. Sens. Sens. Syst.* 7, 43–49.
- Glatz, W., Schwyter, E., Durrer, L., Hierold, C., 2009. Bi₂Te₃-based flexible micro thermoelectric generator with optimized design. *J. Microelectromech. Syst.* 18 (3), 763–772.
- Goldsmid, H., Sheard, A., Wright, D., 1985. The performance of bismuth telluride thermojunctions. *Br. J. Appl. Phys.* 9 (9), 365–370.
- Gongora-Rubio, M., Espinoza-Vallejos, P., Sola-Laguna, L., Santiago-Avilés, J., 2001. Overview of low temperature co-fired ceramics tape technology for meso-system technology (MsST). *Sensors Actuators A* 89 (3), 222–241.
- Gou, R.S.X., Xu, H., Qiu, K., 2017. Dynamic performance analysis of a cascaded thermoelectric generator. *Appl. Energy* 203, 808–815.
- Guan, M., Wang, K., Xu, D., Liao, W., 2017. Design and experimental investigation of a low-voltage thermoelectric energy harvesting system for wireless sensor nodes. *Energy Convers. Manage.* 138, 30–37.
- Haidar, J., Ghobel, J., 2001. Waste heat recovery from the exhaust of low-power diesel engine using thermoelectric generators. In: 20 International Conference on Thermoelectrics, Beijing, China, China.
- Hammel, T., Bennett, R., Otting, W., Fanale, S., 2009. Multi-Mission Radioisotope Thermoelectric Generator (MMRTG) and performance prediction model. In: 7th International Energy Conversion Engineering Conference, Denver, Colorado.
- Hasebe, S., Ogawa, J., Shiozaki, M., Toriyama, T., Sugiyama, S., Ueno, H., Itoigawa, K., 2004. Polymer based smart flexible themopile for power generation. In: 17th IEEE International Conference on Micro Electro Mechanical Systems. Maastricht MEMS 2004 Technical Digest, Maastricht, Netherlands, Netherlands.
- Hayhurst, M., Bitten, R., Mahr, E., Bilardo-Jr, V., 2019. Space Power Heritage Study Final Results. National Aeronautics and Space Administration.
- Hébert, S., 2014. La recherche De Nouveaux matériaux thermoélectriques. *Reflet Phys.* 41, 18–22.
- Holgate, T.-C., Bennett, R., Hammel, T., Caillat, T., Keyser, S., Sievers, B., 2015. Increasing the efficiency of the multi-mission radioisotope thermoelectric generator. *J. Electron. Mater.* 44 (6), 1814–1821.
- Hussain, Q., Brigham, D., Maranville, C., 2009. Thermoelectric exhaust heat recovery for hybrid vehicles. *SAE Int. J. Engines* 2 (1), 1132–1142.
- Huu, T.N., Van, T.N., Takahito, O., 2018. Flexible thermoelectric power generator with Y-type structure using electrochemical deposition process. *Appl. Energy* 210, 467–476.
- Iezzi, B., Ankireddy, K., Twiddy, J., Losego, M., Jur, J., 2017. Printed, metallic thermoelectric generators integrated with pipe insulation for powering wireless sensors. *Appl. Energy* 208, 758–765.
- Intel, 2018. Intel. [Online]. Available: <https://ark.intel.com>. [Accessed 5 1 2019].
- Jeng, T., Tzeng, S., 2013. Technical development of heat energy recovery. *Trans. Canadian Soc. Mech. Eng.* 37 (3), 885–894.
- Jiménez, J., Mánuel, J., Bartsch, H., Breiling, J., García, R., Jacobs, H., Müller, J., Pezoldt, J., Morales, F., 2019. Comprehensive (S)TEM characterization of polycrystalline GaN/AlN layers grown on LTCC substrates. *Ceram. Int.* 45 (7), 9114–9125.
- Kanimbala, E., Pearson, M., Sharp, J., Stokes, D., Priya, S., Tian, Z., 2017. A modeling comparison between a two-stage and three-stage cascaded thermoelectric generator. *J. Power Sources* 365, 266–272.
- Kao, P.-H., Shih, P.-J., Dai, C.-L., Liu, M.-C., 2010. Fabrication and characterization of CMOS-MEMS thermoelectric micro generators. *Sensors* 10 (2), 1315–1325.
- Kim, Y., Gu, H.M., Kim, C., Choi, H., Lee, G., Kim, S., Yi, K., Lee, S., Cho, B., 2018. High-performance self-powered wireless sensor node driven by a flexible thermoelectric generator. *Energy* 162, 526–533.
- Kim, H., Liu, W., Chen, G., Ren, Z., 2015. Relationship between thermoelectric figure of merit and energy conversion efficiency. *Proc. Natl. Acad. Sci. USA* 112 (27), 8205–8210.
- Krzywaniak, A., Proficz, J., Czarnul, P., 2018. Analyzing energy/performance trade-offs with power capping for parallel applications on modern multi and many core processors. In: Proceedings of the 2018 Federated Conference on Computer Science and Information Systems.
- LaGrandeur, J., Crane, D., Hung, S., Mazar, B., Eder, A., 2006. Automotive waste heat conversion to electric power using skutterudite, TAGS, PbTe and Bi₂Te. In: 25th International Conference on Thermoelectrics, Vienna, Austria.
- Lay-Ekuakille, A., Vendramin, G., Trotta, A., Mazzotta, G., 2009. Thermoelectric generator design based on power from body heat for biomedical autonomous devices. In: International Workshop on Medical Measurements and Applications, Cetraro, Italy.
- Leonov, V., 2013. Thermoelectric energy harvesting of human body heat for wearable sensors. *IEEE Sens. J.* 13 (6), 2284–2291.
- Leonov, V., Andel, Y.v., Wang, Z., Vullers, R., Hoof, C.V., 2011. Micromachined polycrystalline Si thermopiles in a T-shirt. *Sensors Transducers* 127 (4), 15.
- Leonov, V., Fiorini, P., Torfs, T., Vullers, R.J.M., Hoof, C.V., 2009. Thermal matching of a thermoelectric energy harvester with the environment and its application in wearable self-powered wireless medical sensors. In: 15th International Workshop on Thermal Investigations of ICs and Systems, Leuven, Belgium.
- Leonov, V., Torfs, T., Kukhar, N.V., Hoof, C.V., Vullers, R.J.M., 2007. Small-size BiTe thermopiles and a thermoelectric generator for wearable sensor nodes. In: Proceedings - 5th European Conference on Thermoelectrics.
- Leonov, V.T.T.C., Vullers, V.H.R., 2009a. Smart wireless sensors integrated in clothing: an electrocardiography system in a shirt powered using human body heat. *Sensors Transducers J.* 107 (8), 165–176.
- Leonov, V., Vullers, R., 2009b. Wearable electronics self-powered by using human body heat: The state of the art and the perspective. *J. Renew. Sustain. Energy* 1.
- Li, Y., Buddharaju, K., Singh, N., Lo, G.Q., Lee, S.J., 2011b. Chip-level thermoelectric power generators based on high-density silicon nanowire array prepared with top-down CMOS technology. *IEEE Electron Device Lett.* 32 (5), 674–676.
- Li, J., Tanaka, S., Umekib, T., Sugimoto, S., Esashi, M., Watanabe, R., 2003. Microfabrication of thermoelectric materials by silicon molding process. *Sensors Actuators A* 108 (1–3), 97–102.
- Li, M., Xu, S., Chen, Q., Zheng, L., 2011a. Thermoelectric-generator-based DC-DC conversion networks for automotive applications. *J. Electron. Mater.* 40 (5), 1136–1143.
- Lind, K., 2017. Understanding the market for implantable medical devices. *Public Policy Inst. (Amer. Assoc. Retired Pers.)* (129), 1–15.
- Liu, S., Hu, B., Liu, D., Li, F., Li, J., Li, B., Li, L., Nan, Y.L.C., 2018a. Micro-thermoelectric generators based on through glass pillars with high output voltage enabled by large temperature difference. *Appl. Energy* 225, 600–610.
- Liu, K., Liu, Y., Xu, Z., Zhang, Z., Yuan, Z., Guo, X., Jin, Z., Tang, X., 2017. Experimental prototype and simulation optimization of micro-radial milliwatt-power radioisotope thermoelectric generator. *Appl. Therm. Eng.* 125, 425–431.
- Liu, C., Pan, X., Zheng, X., Yan, Y., Li, W., 2016. An experimental study of a novel prototype for two-stage thermoelectric generator from vehicle exhaust. *J. Energy Inst.* 89 (2), 271–281.
- Liu, K., Tang, X., Liu, Y., Yuan, Z., Li, J., Xu, Z., Zhang, Z., Chen, W., 2018b. High-performance and integrated design of thermoelectric generator based on concentric filament architecture. *J. Power Sources* 393, 161–168.
- Liu, X., Wu, J., 2019. A method for energy balance and data transmission optimal routing in wireless sensor networks. *Sensors (Basel)* 19 (13).
- Ma, K., Liu, J., 2007. Heat-driven liquid metal cooling device for the thermal management of a computer chip. *J. Phys. D: Appl. Phys.* 40, 4722–4729.
- Máñuel, J., Jiménez, J., Morales, F., Lacroix, B., Santos, A., García, R., Blanco, E., Domínguez, M., Ramírez, M., Beltrán, A., Alexandrov, D., Tot, J., Dubreuil, R., Videkov, V., Andreev, S., Tzaneva, B., Bartsch, H., Breiling, J., Pezoldt, J., Fischer, M., Müller, J., 2018. Engineering of III-Nitride semiconductors on low temperature co-fired ceramics. *Sci. Rep.* 8 (6879).
- Markets, R.a., 2019. Thermoelectric generators market by application (Waste heat recovery, energy harvesting, direct power generation, co-generation), wattage (1kW), temperature (500 °C), material, vertical, component, region - global forecast to 2025. Res. Mark.
- Markowi, P., Prociow, E., Dziedzic, A., 2009. Mixed thick/thin-film thermocouples for thermoelectric microgenerators and laser power sensor. *Opt. Appl.* XXXIX (4), 681–690.
- Markowski, P., 2011. Thick-film photoimageable and laser-shaped arms for thermoelectric microgenerators. *Microelectron. Int.* 28 (3), 43–50.
- Markowski, P., 2014. Thermoelectric energy harvester fabricated in thick-film/LTCC technology. *Microelectron. Int.* 31 (3), 176–185.
- Markowski, P., 2016. Multilayer thick-film thermoelectric microgenerator based on LTCC technology. *Microelectron. Int.* 33 (3), 155–161.
- Markowski, P., Dziedzic, A., 2008. Planar and three-dimensional thick-film thermoelectric microgenerators. *Microelectron. Reliab.* 48, 890–896.
- Markowski, P., Prociów, E., Urbaniak, Ł., 2015. Thermoelectric properties of thin-film germanium-based layers. *Microelectron. Int.* 32 (3), 115–121.
- Markowski, P., Straszewski, L., Dziedzic, A., 2008. Sandwich-type three-dimensional thick-film thermoelectric microgenerators. In: 31st Int. Spring Seminar on Electronics Technology, Budapest, Hungary.
- Mason, L., 2007. Realistic specific power expectations for advanced radioisotope power systems. *J. Propuls. Powe* 23 (5), 1075–1079.
- Mori, M., Yamagami, T., Sorazawa, M., Miyabe, S.T.T., Haraguchi, T., 2011. Simulation of fuel economy effectiveness of exhaust heat recovery system using thermoelectric generator in a series hybrid. *SAE Int. J. Mater. Manuf.* 4 (1), 1268–1276.
- Mostafavi, S., Mahmoudi, M., 2018. Modeling and fabricating a prototype of a thermoelectric generator system of heat energy recovery from hot exhaust gases and evaluating the effects of important system parameters. *Appl. Therm. Eng.* 132, 624–636.
- Musleh, M.A., Topriska, E., Jack, L., Jenkins, D., 2017. Thermoelectric generator experimental performance testing for wireless sensor network application in smart buildings. In: MATEC Web of Conferences, Vol. 120.
- Myers, A., Jur, J., 2017. Effects of thermal energy harvesting on the human – clothing – environment microsystem. In: IOP Conf. Series: Materials Science and Engineering, vol. 254.

- Nurnus, J., 2007. Thermoelectric thin film coolers and generators: novel components for the use in smart systems. In: Smart Systems Integration, European Conference & Exhibition on Integration Issues of Miniaturized Systems - MEMS, MOEMS, ICs and Electronic Components, Berlin, Germany.
- O'Brien, R., Ambrosi, R., Bannister, N., Howe, S., Atkinson, H., 2008. Safe radioisotope thermoelectric generators and heat sources for space applications. *J. Nucl. Mater.* 377, 506–521.
- Olvera, A.A., Moroz, N.A., Sahoo, P., Ren, P., Bailey, T.P., Page, A.A., Uher, C., Poudeu, P.F.P., 2017. Partial indium solubility induces chemical stability and colossal thermoelectric figure of merit in Cu₂Se. *Energy Environ. Sci.* 7, 1–9.
- Orr, B., Akbarzadeh, A., Lappas, P., 2017. An exhaust heat recovery system utilising thermoelectric generators and heat pipes. *Appl. Therm. Eng.* 126, 1185–1190.
- Park, T., Lim, H., Hwang, J., Na, J., Lee, H., Kim, E., 2017. Roll type conducting polymer legs for rigid-flexible thermoelectric generator. *APL Mater.* 5 (7).
- Pasquale, G.D., 2013. 11 - Energy harvesters for powering wireless systems. In: Uttamchandani, D. (Ed.), *Handbook of MEMS for Wireless and Mobile Applications*. Woodhead Publishing, pp. 45–400.
- Patil, D.S., Arakerimath, R.R., Walke, P.V., 2018. Thermoelectric materials and heat exchangers for power generation – A review. *Renew. Sustain. Energy Rev.* 95, 1–22.
- Penella, M.T., Albesa, J., Gasulla, M., 2009. Powering wireless sensor nodes: Primary batteries versus energy harvesting. In: IEEE Instrumentation and Measurement Technology Conference, Singapore.
- Pistioia, G., 2005. Chapter 6 - batteries for medical and special applications. In: *Batteries for Portable Devices*. Elsevier Science B.V., pp. 147–162.
- Proto, A., Bibbo, D., Cerny, M., Vala, D., Kasik, V., Peter, L., Conforto, S., Schmid, M., Penhaker, M., 2018. Thermal energy harvesting on the bodily surfaces of arms and legs through a wearable thermo-electric generator. *Sensors* 18 (6), 1–17.
- Qing, S., Rezania, A., Rosendahl, L., Enkeshafi, A., Gou, X., 2018. Characteristics and parametric analysis of a novel flexible ink-based thermoelectric generator for human body sensor. *Energy Convers. Manage.* 156, 655–665.
- Qualls, A.L., Schmitz, P., Rusick, J.J., Rusick, J.J., Zakrajsek, J.F., Woerner, D.F., Cairns-Gallimore, D., 2017. Dynamic radioisotope power system development for space exploration. In: IEEE Aerospace Conference, Big Sky, Montana.
- Quan, R., Liu, G., Wang, C., Zhou, W., Huang, L., Deng, Y., 2018. Performance investigation of an exhaust thermoelectric generator for military SUV application. *Coatings* 8 (45).
- Risseh, A., Nee, H., Goupil, C., 2018. Electrical power conditioning system for thermoelectric waste heat recovery in commercial vehicles. *IEEE Trans. Transp. Electrif.* 4 (2), 548–562.
- Ritz, F., Peterson, C., 2004. Multi-mission radioisotope thermoelectric generator (MMRTG) program overview. In: Aerospace Conference Proceedings, Big Sky, MT, USA.
- Rosales, J., Chiriac, V., Velez, M., Wang, P., 2018. Energy harvesting device for electronic devices. United States Patent US20180351066A1.
- R.P.S. Committee, 2009. Radioisotope Power Systems: An Imperative for Maintaining U.S. Leadership in Space Exploration. National Academy of Sciences, p. 68.
- Sawires, E.F., Eladawy, M.I., Ismail, Y.I., Abdelhamid, H., 2018. Thermal resistance model for standard CMOS thermoelectric generator. *IEEE Access* 6, 8123–8132.
- Shu, G., Ma, X., Tian, H., Yang, H., Chen, T., Li, X., 2018. Configuration optimization of the segmented modules in an exhaust-based thermoelectric generator for engine waste heat recovery. *Energy* 160, 612–624.
- Siddique, A., Mahmud, S., Heyst, B., 2017. A review of the state of the science on wearable thermoelectric power generators (TEGs) and their existing challenges. *Renew. Sustain. Energy Rev.* 73, 730–744.
2019. Sigma-Aldrich. [Online]. Available: <https://www.sigmaaldrich.com/germany.html>. [Accessed 11 2019].
- Simon, R., 1961. Maximum figure of merit of thermoelectric materials. *Adv. Energy Convers.* 1, 81–92.
- Singh, G., 2007. FY 2007 Progress Report For AdvAnced Combustion Engine Technologies. Alliance Technical Services, Inc., Oak Ridge.
- Snyder, G., 2004. Application of the compatibility factor to the design of segmented and cascaded thermoelectric generators. *Appl. Phys. Lett.* 84 (13), 2436–2438.
- Snyder, G.S., Snyder, A.H., 2017. Figure of merit ZT of a thermoelectric device defined from materials properties. *Energy Environ. Sci.* 11, 1–6.
- Snyder, G., Ursell, T., 2003. Thermoelectric efficiency and compatibility. *Phys. Rev. Lett.* 91 (14), 148301–148305.
- Solbrekken, G., Yazawa, K., Bar-Cohen, A., 2004. Thermal management of portable electronic equipment using thermoelectric energy conversion. In: The Ninth Intersociety Conference on Thermal and Thermomechanical Phenomena in Electronic Systems (IEEE Cat. No.04CH37543), Las Vegas, NV, USA, USA.
- Stark, I., 2011. Converting body heat into reliable energy for powering physiological wireless sensors. In: WH '11 Proceedings of the 2nd Conference on Wireless Health, San Diego, California, USA.
- Streb, A., 1966. Radioisotope power systems for manned space stations. *Progress Astronaut. Rocket.* 16, 3–29.
- Suarez, F., Parekh, D., Ladd, C., Vashaee, D., Dickey, M.D., 2017a. Flexible thermoelectric generator using bulk legs and liquid metal interconnects for wearable electronics. *Appl. Energy* 202, 736–745.
- Suarez, F., Parekh, D., Ladd, C., Vashaee, D., Dickey, M., Öztürk, M., 2017b. Flexible thermoelectric generator using bulk legs and liquid metal interconnects for wearable electronics. *Appl. Energy* 202, 736–745.
- Suski, E., 1995. Method and apparatus for recovering power from semiconductor circuit using thermoelectric device. US Patent US5419780A.
- Tang, Z., Deng, Y., Su, C., Shuai, W., Xie, C., 2015. A research on thermoelectric generator's electrical performance under temperature mismatch conditions for automotive waste heat recovery system. *Case Stud. Therm. Eng.* 5, 143–150.
- Temizer, İ., İlkiç, C., 2016. The performance and analysis of the thermoelectric generator system used in diesel engines. *Renew. Sustain. Energy Rev.* 63, 141–151.
- Thelemann, T., Thust, H., Hintz, M., 2002. Using LTCC for microsystems. *Microelectron. Int.* 19 (3), 19–23.
- Thielen, M., Sigrist, L., Magno, M., Hierold, C., Benini, L., 2017. Human body heat for powering wearable devices: From thermal energy to application. *Energy Convers. Manage.* 131, 44–54.
- Tian, H., Jiang, N., Jia, Q., Sun, X., Shu, G., Liang, X., 2015. Comparison of segmented and traditional thermoelectric generator for waste heat recovery of diesel engine. *Energy Procedia* 75, 590–596.
- Tomita, M., Oba, S., Himeda, Y., Yamato, R., Shima, K., Kumada, T., Xu, M., Takezawa, H., Mesaki, K., Tsuda, K., Hashimoto, S., Zhan, T., Zhang, H., Kamakura, Y., Suzuki, Y., Inokawa, H., Ikeda, H., Matsukawa, T., Matsuki, T., Watanabe, T., 2018. 10 μW/cm²-Class high power density planar si-nanowire thermoelectric energy harvester compatible with CMOS-VLSI technology. In: Symposium on VLSI Technology, Honolulu, HI, USA.
- Torfs, T., Leonov, V., Hoof, C., Gyselinckx, B., 2006. Body-heat powered autonomous pulse oximeter. In: Sensors, Daegu, South Korea.
- Torfs, T., Leonov, V., Vullers, R., 2007. Pulse oximeter fully powered by human body heat. *Sensors Transducers* 180 (6), 1230–1238.
- Tuna, G., Gungor, V., 2016. 2 - Energy harvesting and battery technologies for powering wireless sensor networks. In: Kolavennu, R.B.A.S. (Ed.), *Industrial Wireless Sensor Networks*. Woodhead Publishing, pp. 25–38.
- U.E.I. Administration, 2018. Short-Term Energy Outlook (STEO) 2018, US.
- Völklein, F., Megier, A., 2006. Thermoelectric micromechanical systems. In: Rowe, D.M. (Ed.), *Thermoelectrics Handbook: Macro to Nano*. CRC Press.
- Völklein, F., Min, G., Rowe, D., 1999. Modelling of a microelectromechanical thermoelectric cooler. *Sensors Actuators A* 75 (2), 95–101.
- Wahbah, M., Alhwari, M., Mohammad, B., Saleh, H., Ismail, M., 2014. Characterization of human body-based thermal and vibration energy harvesting for wearable devices. *IEEE J. Emerg. Sel. Top. Circuits Syst.* 4 (3), 354–363.
- Wang, W., Cionca, V., Wang, N., Hayes, M., O'Flynn, B., O'Mathuna, C., 2013. Thermoelectric energy harvesting for building energy management wireless sensor networks. *Int. J. Distrib. Sens. Netw.* 9 (6).
- Wang, Z., Leonov, V., Fiorini, P., Hoof, C.V., 2009. Realization of a wearable miniaturized thermoelectric generator for human body applications. *Sensors Actuators A* 156 (1), 95–102.
- Watanabe, T., Asada, S., Xu, T., Hashimoto, S., Ohba, S., Himeda, Y., Yamato, R., Zhang, H., Tomita, M., Matsukawa, T., Kamakura, Y., Ikeda, H., 2017. A scalable Si-based micro thermoelectric generator. In: Electron Devices Technology and Manufacturing Conference (EDTM 2017), Toyama, Japan.
- Werner, J., Johnson, S., Dwight, C., Lively, K., 2016. Cost comparison in 2015 dollars for radioisotope power systems—Cassini and Mars science laboratory. In: The INL is a U.S. Department of Energy National Laboratory Operated by Battelle Energy Alliance.
- Wilbrecht, S., Beitschmidt, M., 2018. The potential of a cascaded TEG system for waste heat usage in railway vehicles. *J. Electron. Mater.* 47 (6), 3358–3369.
- Wu, H., Zhao, L., Zheng, F., Wu, D., Pei, Y., Tong, X., Kanatidis, M., He, J., 2014. Broad temperature plateau for thermoelectric figure of merit ZT42 in phase-separated PbTe0.75O₃. *Nature Commun.* 5 (4515), 1–9.
- Yan, J., Liao, X., Ji, S., Zhang, S., 2019. MEMS-based thermoelectric-photoelectric integrated power generator. *J. Microelectromech. Syst.* 28 (1), 1–3.
- Yang, J., 2005. Potential applications of thermoelectric waste heat recovery in the automotive industry. In: 24th International Conference on Thermoelectrics, Clemson, SC, USA, USA.
- Yang, Y., Wei, X., Liu, J., 2007. Suitability of a thermoelectric power generator for implantable medical electronic devices. *J. Phys. D: Appl. Phys.* 40 (18), 5790–5800.
- Yang, M.-Z., Wu, C.-C., Dai, C.-L., Tsai, W.-J., 2013. Energy harvesting thermoelectric generators manufactured using the complementary metal oxide semiconductor process. *Sensors* 13, 2359–2367.
- Yu, C., Chau, K., 2009. Thermoelectric automotive waste heat energy recovery using maximum power point tracking. *Energy Convers. Manage.* 50, 1506–1512.
- Yuan, Z., Tang, X., Liu, Y., Xu, Z., Liu, K., Li, J., Zhang, Z., Wang, H., 2019. Improving the performance of a screen-printed micro-radioisotope thermoelectric generator through stacking integration. *J. Power Sources* 414, 509–516.

- Yuan, Z., Tang, X., Xu, Z., Li, J., Chen, W., Liu, K., Liu, Y., Zhang, Z., 2018. Screen-printed radial structure micro radioisotope thermoelectric generator. *Appl. Energy* 225, 746–754.
- Zhang, Y., Cleary, M., Wang, X., Kempf, N., Schoensee, L., Yang, J., Joshi, G., Meda, L., 2015. High-temperature and high-power-density nanostructured thermoelectric generator for automotive waste heat recovery. *Energy Convers. Manage.* 105, 946–950.
- Zhang, L., Tosho, T., Okinaka, N., Akiyama, T., 2008. Design of cascaded oxide thermoelectric generator. *Mater. Trans.* 49 (7), 167561680.
- Zhang, H., Xu, T., Hashimoto, S., Watanabe, T., 2018. The possibility of mW/cm²-class on-chip power generation using ultrasmall Si nanowire-based thermoelectric generators. *IEEE Trans. Electron Devic*s 65 (5), 2016–2023.
- Zhao, X., Han, W., Zhao, C., Wang, S., Kong, F., Ji, X., Li, Z., Shen, X., 2019. Fabrication of transparent paper-based flexible thermoelectric generator for wearable energy harvester using modified distributor printing technology. *ACS Appl. Mater. Interfaces* 11 (10), 10301–10309.
- Zhou, Y., Paul, S., Bhunia, S., 2008. Harvesting wasted heat in a microprocessor using thermoelectric generators: Modeling, analysis and measurement. In: *Design, Automation and Test in Europe*, Munich, Germany.
- Zhu, J., Xu, Z., Jia, L., 2018. Design and fabrication of 3D flexible thermoelectric energy generator using chemical vapor deposition method based on paper substrate. In: *International Symposium in Sensing and Instrumentation in IoT Era (ISSI)*, Shanghai, China.
- Ziouche, K., Yuan, Z., Lejeune, P., Lasri, T., Leclercq, D., Bougrioua, Z., 2017. Silicon-based monolithic planar micro thermoelectric generator using bonding technology. *J. Microelectromech. Syst.* 26 (1), 45–47.